Title: ***Aerodynamics characteristics of butterfly flight through measurement of three-dimensional unsteady velocity field using TR-PIV system***

REF: AOARD-09-4102
Contract No. FA23860914102

PI: Debopam Das
Debopam Das; Ph. D.
Associate Professor
Department of Aerospace Engineering
Indian Institute of Technology Kanpur
Phone: +91 512 259 6163 /7227 /8578
Email: das@iitk.ac.in; [redacted]

Problem definition

The present work is divided into two major portions. One being the flow visualization and PIV measurements the other is force measurement. In the force measurements the effect of parameters like wings size and flapping frequency is studied. For the PIV measurements the wake profile, the vortex interactions and other flow features that takes place in such flapping flight are studied. In the flow visualization carried out in water, the basic flow physics has been observed and found to justify with the PIV results in the same Reynolds number range <5000. Initially some suitable flapping models are chosen and both the experiments of force and PIV measurements are carried out in no forward velocity, thus shifting the level of study to completely unsteady regime (advance ratio<1). Finally the observations with the PIV analysis are compared with the force results to explain the nature of the forces and their patterns. Thus PIV experiments serve both as a tool of flow visualization as well as a quantitative judgment for studying the nature of flow over a flapping wing.

Introduction

Large lift generation capacity and efficient flying of natural flying objects has generated enormous amount of interest among scientists and engineers for decades. The intricate 3D unsteady motions of wings have made this study complex. However with the advancement of technology and improvements in experimental techniques the physics behind such flight can be much better understood than before. The application of uncovering the knowledge of physics of such flapping flight can be of significant interest while designing flying robots or MAVs (Micro Air vehicles) of flapping wing type. Though MAVs of fixed wing have been successfully made and implemented as it uses the same conventional aerodynamics of steady state, whereas flapping wing flight is still not clearly understood. The basic aerodynamics fails while accounting for the mechanisms or forces generated by flapping wing fliers as the existing theories are limited by the steady state hypothesis whereas the flapping flight is completely unsteady in nature and thus complicated three dimensional unsteady effects comes into picture and make the study complex.

Report Documentation Page

Form Approved
OMB No. 0704-0188

1. REPORT DATE	2. REPORT TYPE	3. DATES COVERED
19 NOV 2009	**FInal**	**01-08-2008 to 01-07-2009**

4. TITLE AND SUBTITLE
Aerodynamics characteristics of butterfly flight through measurement of three-dimensional unsteady velocity field using

5a. CONTRACT NUMBER
FA23860814082

5b. GRANT NUMBER

5c. PROGRAM ELEMENT NUMBER

6. AUTHOR(S)
Das Debopam

5d. PROJECT NUMBER

5e. TASK NUMBER

5f. WORK UNIT NUMBER

7. PERFORMING ORGANIZATION NAME(S) AND ADDRESS(ES)
Indian Institute of Technology Kanpur,IIT Kanpur, Kanpur, UP 208016,India,IN,208016

8. PERFORMING ORGANIZATION REPORT NUMBER
N/A

9. SPONSORING/MONITORING AGENCY NAME(S) AND ADDRESS(ES)
AOARD, UNIT 45002, APO, AP, 96337-5002

10. SPONSOR/MONITOR'S ACRONYM(S)
AOARD

11. SPONSOR/MONITOR'S REPORT NUMBER(S)
AOARD-084082

12. DISTRIBUTION/AVAILABILITY STATEMENT
Approved for public release; distribution unlimited

13. SUPPLEMENTARY NOTES
This is an interim report as the project was renewed with a new contract, reference AOARD #094102.

14. ABSTRACT
This report investigates understanding insect flight (having flapping and feathering motion) in view of lift & thrust generation, essential for flight control, with simultaneous measurement of velocity and forces. The present work is divided into two major portions. One being the flow visualization and PIV measurements, the other is force measurement.

15. SUBJECT TERMS
Fluid Dynamics, Aerodynamic Design and Analysis

16. SECURITY CLASSIFICATION OF:			17. LIMITATION OF ABSTRACT	18. NUMBER OF PAGES	19a. NAME OF RESPONSIBLE PERSON
a. REPORT	b. ABSTRACT	c. THIS PAGE			
unclassified	**unclassified**	**unclassified**	**Same as Report (SAR)**	**42**	

Mechanisms responsible for unusually high generation of lift in the unsteady regime of consideration are discussed in this section. These mechanisms have been observed and studied but the replication of any of these into real scenario of MAVs have not been into much of progress yet. Still a lot of things are not fully understood. Even there exist several theories about the mechanisms and the subsequent lift generation which are mainly divided into the following.

Unsteady Leading Edge Vortex (LEV)

As air passes around the sharp leading edge of an insect wing, it breaks away from the wing and rolls up into a leading-edge vortex (LEV). LEV is a region of low pressure above the wing, and this provides an extra suction that increases the lift. LEVs are not new to aerodynamics, and indeed they keep delta-winged aircraft like Concorde and many other Fighter jet planes up in the air, where the LEVs are generated passively by the swept leading edge of the wing. What is unexpected and amazing about insect flight is that the LEVs are created and stabilised by the flapping motion itself. What would have been expected is as the LEV forms, the flow should continue to feed into the LEV. This would normally cause the vortex to grow so large that it breaks away from the wing, normalizing the low pressure zone, ruining the lift, and stalling the wing. However, it has been discovered that the flapping motion causes the LEV to spiral out to the wingtip, siphoning off the vortex and delaying the stall. The augmented lift, coupled with the delayed stall, is the principle mechanism that insects use for generating lift. It has been shown in this study as well, that this LEV stays in the total downstroke and even in some part of the upstroke when it should have been dispersed and dissolved. LEV accounts for 60-70% of the total lift generated as reported earlier in the literature.

The reasons of this delayed stall and stabilization of this LEV is explained by many theories. Three distinct categories of insect LEV structure have been described on the basis of studies with real insects and mechanical flapping models (Rayner, 1979). These three categories of LEV are summarized in Fig.1. The differences between these flow-fields are non-trivial. The three categories of LEV have qualitatively different flow topologies, corresponding to qualitatively different local solutions to the Navier–Stokes equations (Thomas et al., 2004). Moreover, because the topology of the vortex differs qualitatively between the three categories of LEV structure, the overall size of the vortex and its contribution to the total lift generated by the model/insect can only be calculated correctly if the correct topology is used.

ROTATIONAL LIFT

When an insect reaches the end of the upstroke, it must rotate its wings to place them at the correct angle of attack for the start of the downstroke. Similarly, the wings must flip over between the downstroke and upstroke. This is to take advantage of the interaction among the various vertical structures developed over and below the wing and enhance or delay any shedding. Ellington first suggested in 1984 that these rapid rotations could produce extra lift, drawing on some experimental and theoretical results for aeroplane wings with rapidly increasing angles of attack. Michael Dickinson's group, working at

Berkeley with a mechanical model of a fruit fly, clearly demonstrated this effect in 1999. Not only is this lift important for weight support, but it is also a potent mechanism for flight control. Dickinson speculates that fruit flies generate steering torques by carefully adjusting the timing of wing rotation at the stroke transitions. The same has been observed in the present study even later discussed.

WAKE CAPTURE

Insects generate lift and thrust by producing and shedding vortices from their wings. These vortices move with the wake as spiralling masses of air that slowly decay and disappear, rather like the tip vortices of aeroplanes. For insects with high wingbeat frequencies, such as flies, the vortices move only a short distance before the wing returns in the cycle, and they can use this as a point of leverage for generating additional lift.

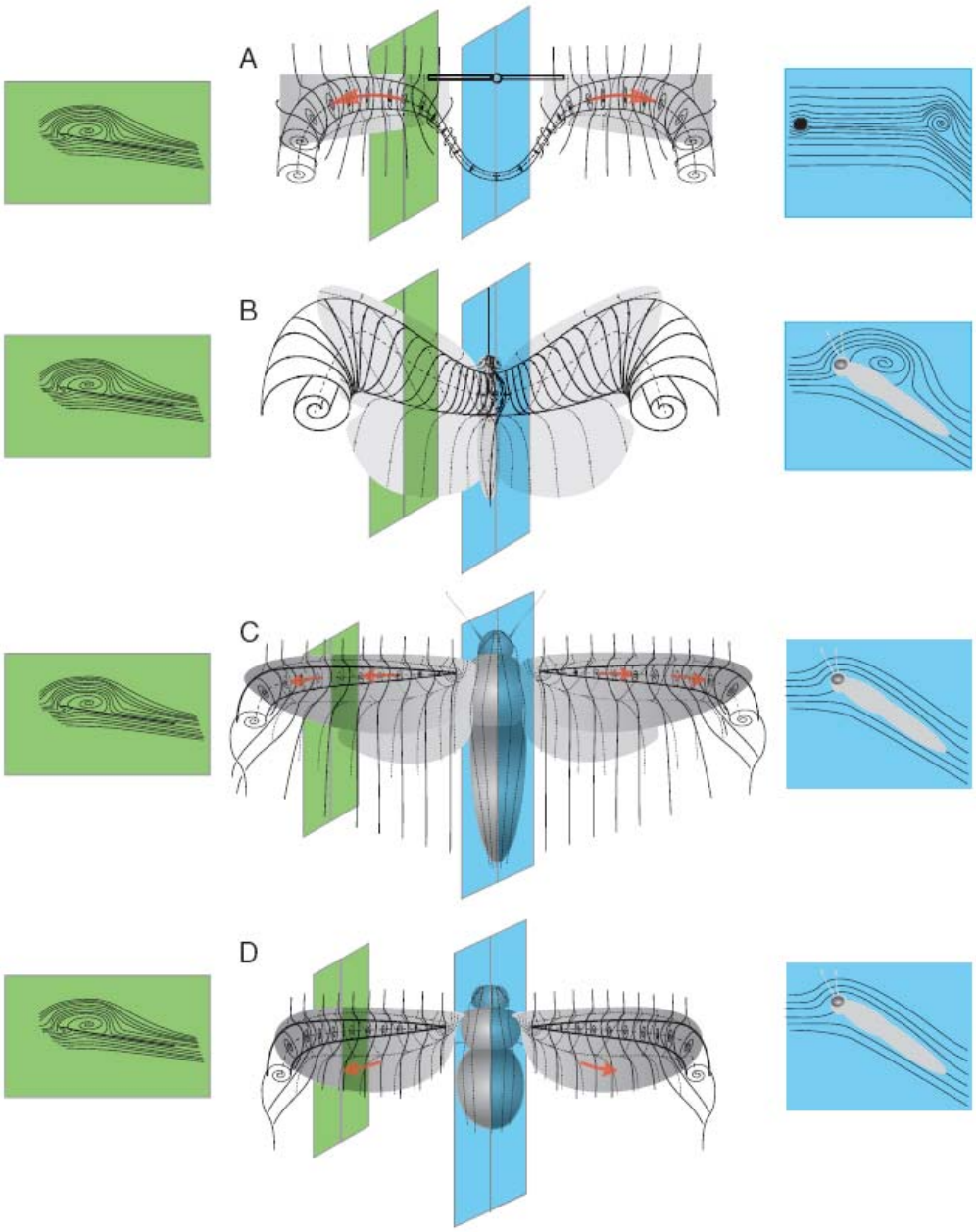

Figure1.1 (taken from R J Bomphrey et al, 2004) (A) Class I: The LEV inflects into tip and root vortices on each wing. The tip vortices connect to form a vortex ring behind the model, and the root vortices also connect so that the wake consists of one continuous vortex loop of complex shape. (B) Class II: LEV extending across the thorax of a hawkmoth and inflecting to form both tip vortices. There is no significant spanwise flow. (C) Class III: the structure described by Ellington and colleagues (Ellington et al., 1996; Van den Berg and Ellington, 1997a). In this model there must be a surface-bound focus at the base of each wing and attached flow over the thorax. (D) Also Class III: the flow, topologically similar to C, scaled for *Drosophila* by Birch and Dickinson (2001).

This process of ‘wake capture’, described by Dickinson's group in 1999, is another mechanism that fruit flies use for generating extra lift. This mechanism, unlike the LEV, might not be a widespread phenomenon because it needs a relatively high wing beat frequency. But it does suggest that other mechanisms whereby vortices interact might be useful for generating lift or torques for steering. Apart from this these shed vortices are high energy containing structures which are utilized back again in the subsequent stroke as the wing comes back before these vortices could move along with the wake. This saves power and enhances the flapping efficiency. The disturbance and unsteadiness the wing generates, it passes over the same again and again saving the effort required and produces some lift and thrust as well. Current research is investigating insects with two pairs of wings (forewings and hindwings) such as locusts and dragonflies. The forewings produce and shed vortices and their interaction with the flapping hindwings and the vortices that they are creating is not yet understood.

CLAP AND FLING

This mechanism has been extensively been studied by Weis-Fogh (1973). As the terminology suggests, it advantageously makes use of the interaction between two wings as they near each other at the extreme ends of the stroke, providing that the total flapping angle is nearly 180^{o}. Fig 1.2 depicts the wing kinematics and the consequent vortex development for a clap and fling motion.

The wing surfaces press together at the end of the upstroke for an extended period of time, mimicking a motion much like two hands coming together for a clap. As the wings separate and open for the next downstroke, they rotate around their trailing edges. The trailing edges remain adjacent and connected together until the included angle reaches 120^{o}. At this instant, the wings form a V-shape before they begin parting away from each other. The sudden translation of opposing section causes air to rush into the widening gap and produce high strength vortices of equal and opposite sign. This leads to a large circulation and lift in the wing without the negatives of vortex shedding since the total circulation around both wings remains zero. Significant amount of work has been done by people over this clap and fling mechanism and the fluid dynamics underneath it [15]. Again this clap and fling helps in the sustaining of lift in the upstroke by vortex ejections twice at the start and end of the clap mechanism, the details of which shall be discussed later in chapter 3. In this study also the same is being used in the experimental model.

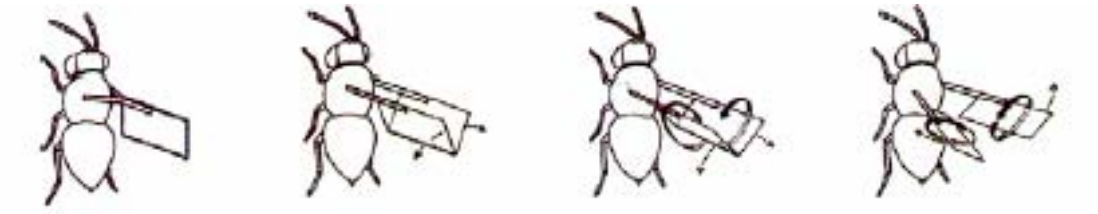

Figure 1.2 Clap and fling mechanism for housefly (Ref. C P Ellington, 1999)

2. Experimental set up

The aim of the experiments conducted is to understand the nature of flapping flight through measurements of velocity field and aerodynamic forces generated in the flapping process. The forces generated are reasoned and justified through the visualization of flowfield through PIV results. The growth of LEV is intended to be studied. Thus the PIV experiments are to be performed at different chord sections of each wing to find out the class of LEV involved in this particular case. Again the difference across the different sections of a wing is observed and repeatability is checked out to be sure of the results. The same process is repeated for other wings as well so as to figure out any difference in the flowfield or timing of any significant mechanism with the change in wing size or the flapping frequency. For the force measurement, once the model is set up with load cell, only wing change and frequency variation is required for force study. Whereas for PIV measurements a partially closed container of glass or any other transparent material on 2sides is used to check the amount of smoke around the wing nearly same every time lending the control over the seeding particle density which has to be maintained at an uniform level for getting good data. The amount of smoke to be filled in the chamber, the settling time provided to get rid of any unwanted velocities that might be present during injection of smoke, has to be learnt out of hit and trial and the best possible trial has to be repeated further for experiments. Again for the general understanding of the nature of flowfield some visualization experiments are conducted in water to check the dependency on the flowfield on the same Reynolds number range.

Models

For our experiments of force and PIV measurements three different models have been used. Proper study of the flow properties and the flow field as a whole will not be appropriate until the models are well made with different degrees of freedom with the close simulation of the real case or near resemblance to natural fliers. Here the model resemblance is with the monarch butterflies thus the flapping angle, time of flapping cycle, range of flapping frequencies and size of the wing are made close to the real monarch butterfly. Though there are many forms and types of butterfly found in nature varying in types and shapes and flying parameters, monarch is chosen which uses a clap and fling mechanism with total flapping angle around 90^0. The same has been incorporated in the model as such. Wing is made of Mylar membrane which is scaled as per the wing of an average monarch butterfly (Fig2.1). Then two more scaled sizes are made to account for the variation in lift and thrust with wing size. Two other models have been chosen to study the effects of feathering and lagging in addition to flapping.

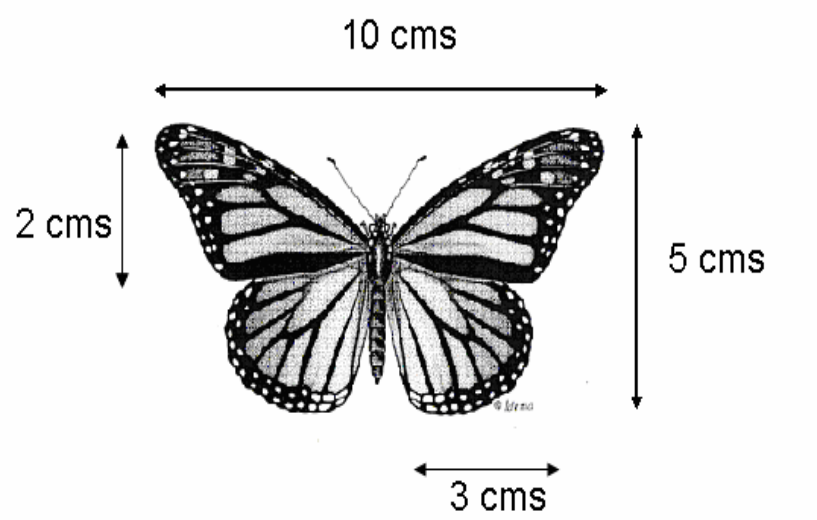

Figure 2.1 1X model of the monarch butterfly wing with dimensions.

Model 1

The first model simulates flapping motion with a 4 bar quick-return mechanism as shown in Fig 2.2. It has only one degree of freedom of flapping with time difference in the two strokes (downstroke and upstroke) of the flapping cycle. The time ratio is 1.3 where downstroke is slower. The reason to choose a flapping mechanism with a relatively larger downstroke time is chosen based on the observed flight patterns of flying animals with advance ratio J <1 such as bats and certain insects. Usually the maximum time ratio is 1:2 and it varies with the speed of flight and hence species (Hendrick et al, 2002 and Tobalske et al, 2003). The wing leading edge is glued to the flapping linkage arm with which it flaps as shown in Fig 2.2. The free end of the wing deflects a little during flapping motion adding to the feathering effect. The bigger the wing the more feathering it undergoes. For the wings we have considered the feathering angle that comes into play is less. But a little change in feathering angle also changes the dynamics of the force generation considerably as discussed in chapter 3. The insect model wing is a scaled model of monarch butterfly with a 1X (corresponds to the original size shown in Fig 2.1.), 1.5X and 1.75X (1.5 and 1.75 times of 1X model in span and chord wise directions). Force measurements are carried out for all three wings and PIV experiments are performed with the largest and smallest wing.

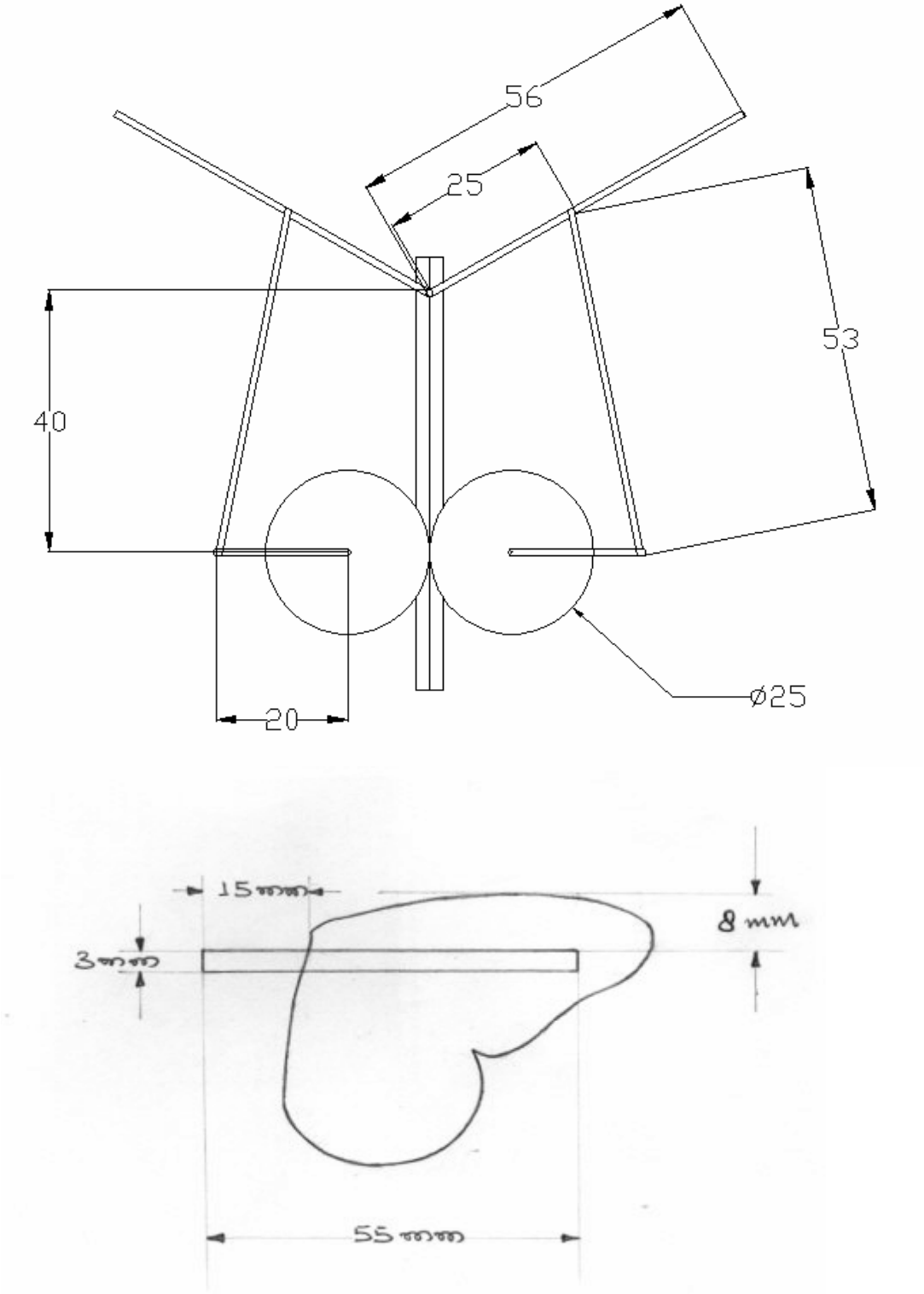

Figure 2.2 Schematic view of model 1 and wing mounting (all units in mm)

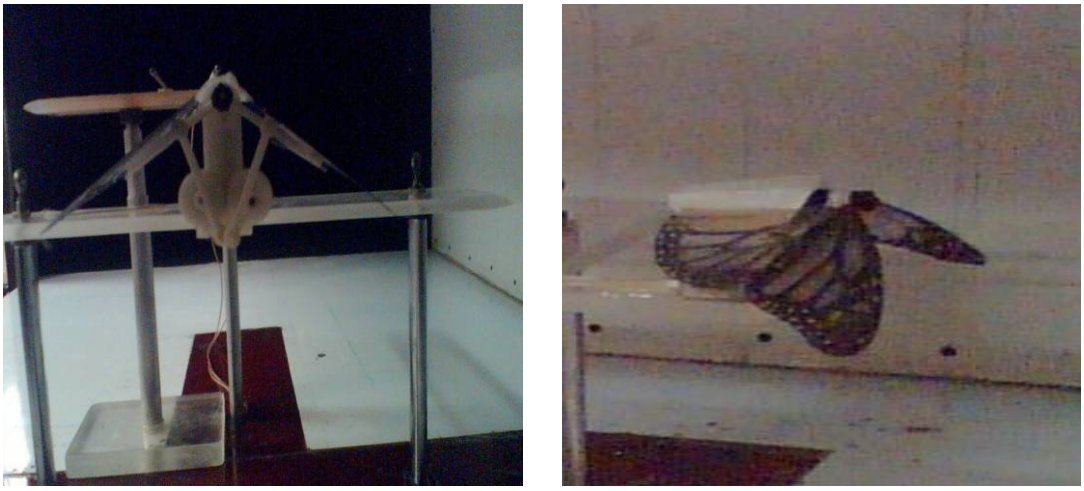

Figure 2.3 Model 1 with 1.75X wings on it.

Model 2

The effect of flapping (clap and fling) motion has been incorporated in the model 1. In the model 2, effect of feathering is incorporated in the mechanism and the wing undergoes both flapping and feathering by the linkage mechanism itself (see Fig.2.4). Here the wing is fixed in a frame and thus there is no feathering effect due to deflection. The feathering effects are obtained by the mechanism alone. The model 2 is made with less angle of flapping so as to study the effect of the net angle of flapping if any on the flowfield. Due to structural changes and requirement of a high torque motor to overcome the resistance in the feathering part of the mechanism, the model is bigger and heavier. Hence force measurements are not done with this model as the force limitations of the load cell is 1 Kg. Only PIV experiments are carried out with this model.

Model 3

Apart from flapping and feathering, lagging motion is also incorporated in the 3rd model. This is again a miniature model, so weight of the model being less the force experiments are performed with this model. Here, even the same wings are used as done with model 1. But due to feathering and lagging motion the net swept angle of flapping became very large. PIV experiments being limited to the area on which measurements can be taken, PIV experiments are not performed with this model. Just the force estimation is done with load cells, so as to make out whether the lagging effect is making any change in the forces generated. PIV experiments can be carried out with the existing system by covering different parts of flow field separately with some overlapping zone and taking a union of the data of different zones. But such experiments with the unsteady flow requires phase synchronization and hence, more effort and time.

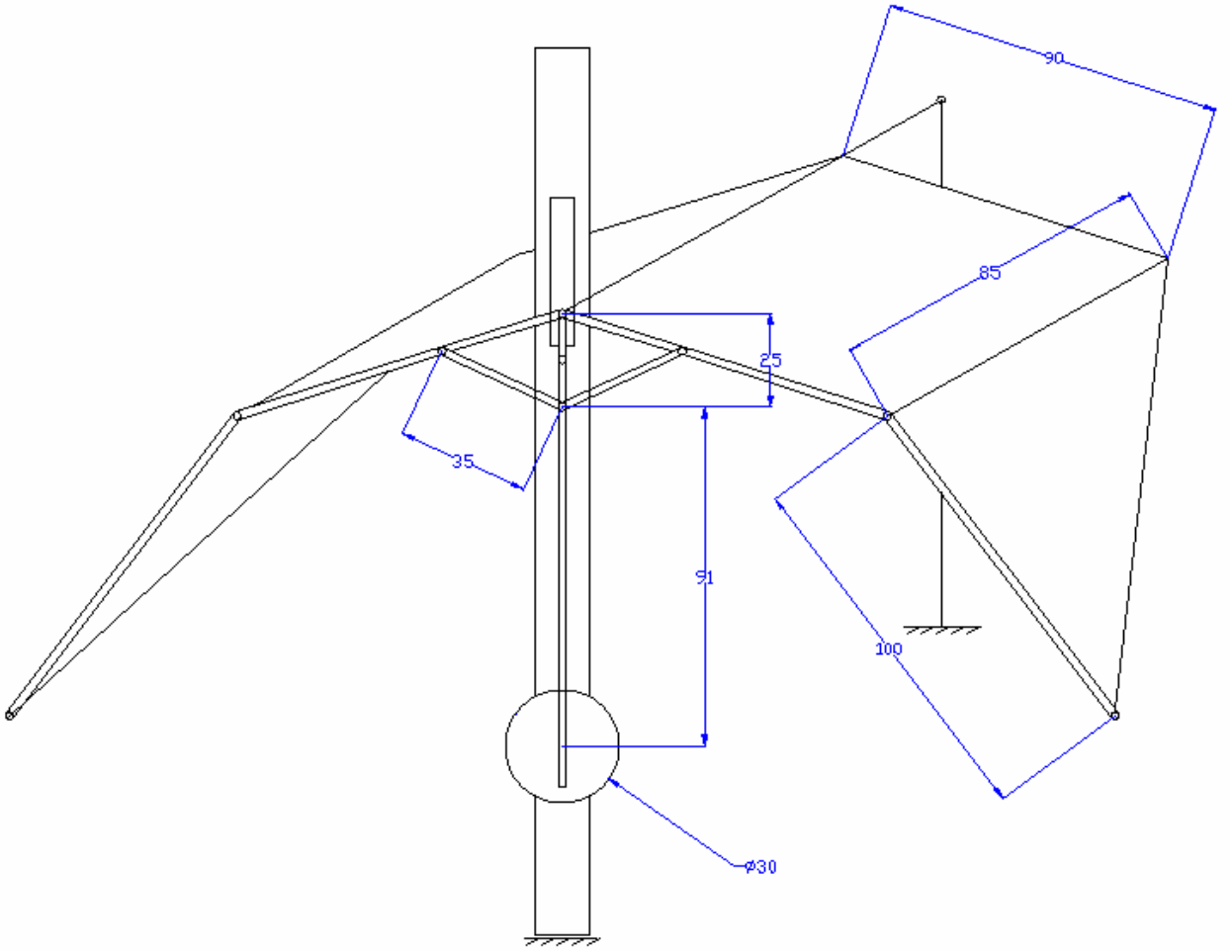

Figure 2.4 Schematic diagram of model 2 (all units are in mm)

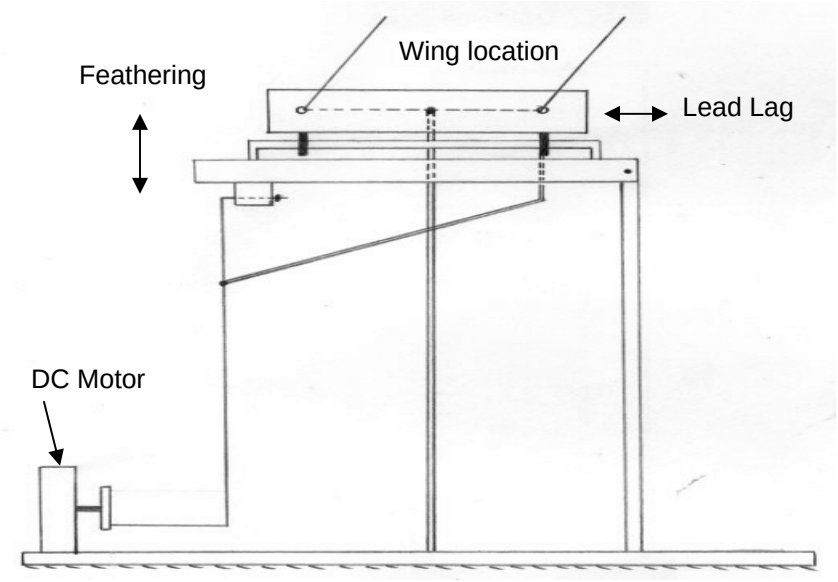

Figure 2.5 schematic view of model 3

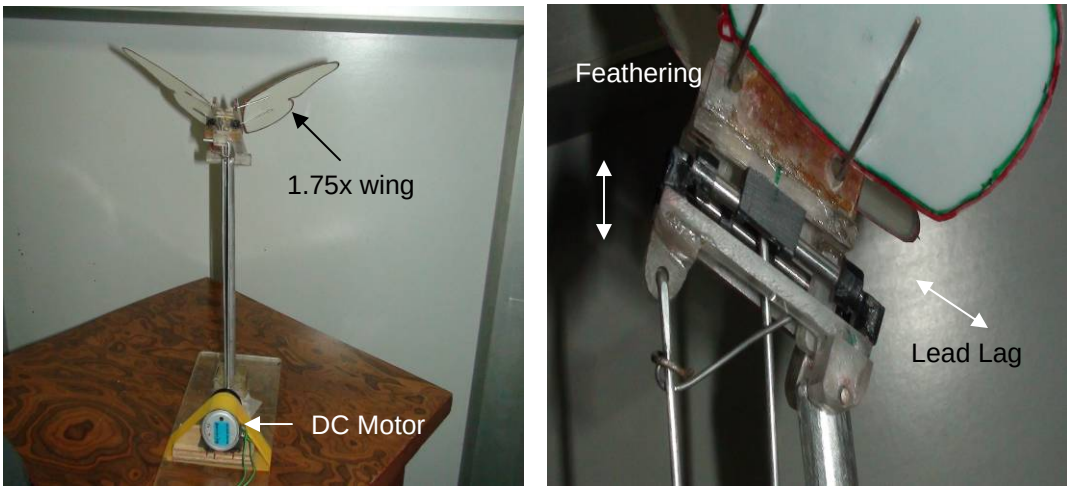

Figure 2.6 Model 3 with lead lag motion with 1.75X wing on it.

PIV measurements

The experiments are carried out in a closed chamber of glass or thermocoil depending upon the size of the model as a whole. Model 1 is fitted with monarch butterfly's scaled wings (Fig2.1). Measurements are carried out in cross-sectional planes along the chord of the wing in different spanwise locations. The flapping frequency is kept constant (4Hz for 1.75X, 6Hz for 1X wing) during experiments at different sections. The size of the wing is varied on the insect model to study the effect of size and the frequency of flapping. As the wings are connected by linkages to a dc motor, the current and voltage supplied to the motor are kept constant, thus the change of wing size automatically changes the frequency of flapping at the same time.

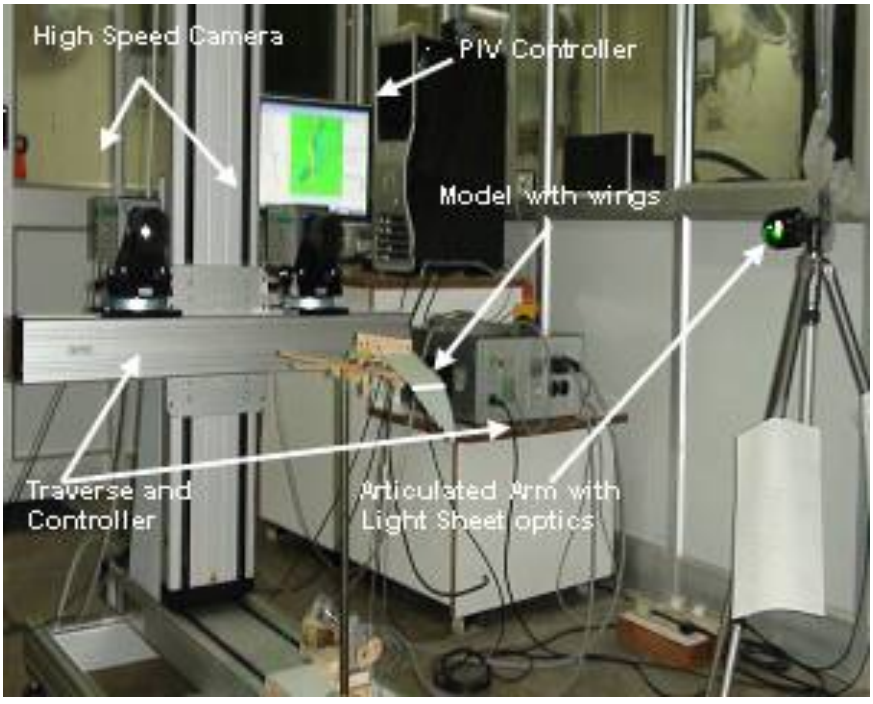

Figure 2.7 Experimental set up with laser, camera and the model

A double pulsed Nd: YAG laser (Quanta system, 200mJ/pulse, 10Hz) is used for illuminating the flow field. PIV mmeasurements are carried out at 10Hz acquisition frequency.The enclosed chamber is filled with smoke containing the seeding particles. The size of the seeding particles is ≈1μm. The time between the two laser pulses is kept as 978μs for measurements. A Nanosense Mk III (1000 frames/sec, 1280x1024 resolution) camera is used for capturing the particle images, run in dual frame mode with the same timed delay as the two lasers. Laser and camera are synchronized by a timer box which is controlled by the computer software. The velocity and vorticity variations of the flow field are calculated for different experiments using Dynamic Studio software from DANTEC dynamics.

Though during the PIV experiments the smoke containing the seeding particle may have some forward velocity depending upon the way of applying it, yet it is negligible enough to be accounted for in the short span of the experiments performed. To overcome the chance of smoke having some forward velocity, some settling time has been kept for the smoke to get stabilized in the chamber containing the model, before the measurements are finally done. Thus the unsteady regime can be ensured. The smoke quantity, the settling time and the way of putting it is purely based on hit and trial and after finding the best possible way, the same is repeated for all the experiments of PIV.

Measurements are taken at 3 sections at the wing. For the 1X model, the measurements are carried out at 0.2R, 0.3R, and 0.5R respectively from the tip of the wing, where R is the single wing span (Fig2.1). For the 1.75X (1.75 times the size of 1X model) measurements are taken at 0.3R, 0.4R, and 0.6R respectively from the tip of the wing.

Force measurement

Force measurements are carried out by placing the model over a two component platform balance. Load cells are connected to a signal conditioner (Fig2.6) which is finally connected to the computer using the NI 4472 card. A lab view interface program is used for acquisition of the signals. The program mainly acquires voltage readings from the load cell which is calibrated to forces using known weights.

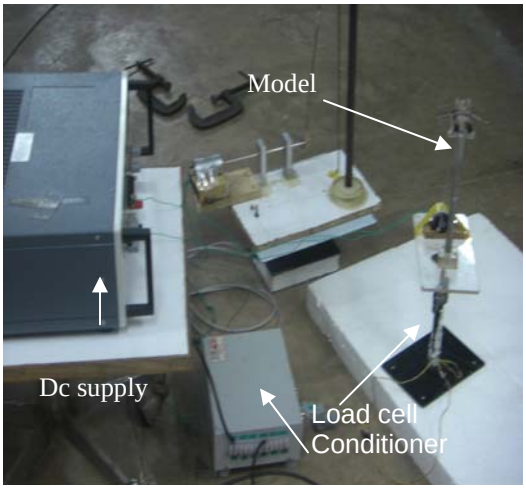

Figure 2.8 the experimental set up for force measurements

Flow visualization in water

To understand the complex unsteady mechanism of unusually high force generation through flapping wing, flow visualization experiments were carried out. Flow features of such unsteady flow are usually complex and dominated with vortical structures. Efforts have been made to visualize such vortex dominated flow and understand its role in flapping flight. Experimental setup and flow visualization is described in this section.

All the visualization experiments were conducted in a water tank made of 6mm glass and Perspex sheets. A light sheet was used to illuminate a particular plane of the flow field in study. A video camera (SONY DCR-VX2100E PAL) (25 frames/s) is mounted on top of the setup in such a way that it is perpendicular to the light sheet and captures the entire phenomenon in that plane. The schematic sketch is shown in Figs 2.9 and 2.10. The flapping wing mechanism is placed on the tank in such a way that the wing is completely immersed in water, even at the end stroke position.

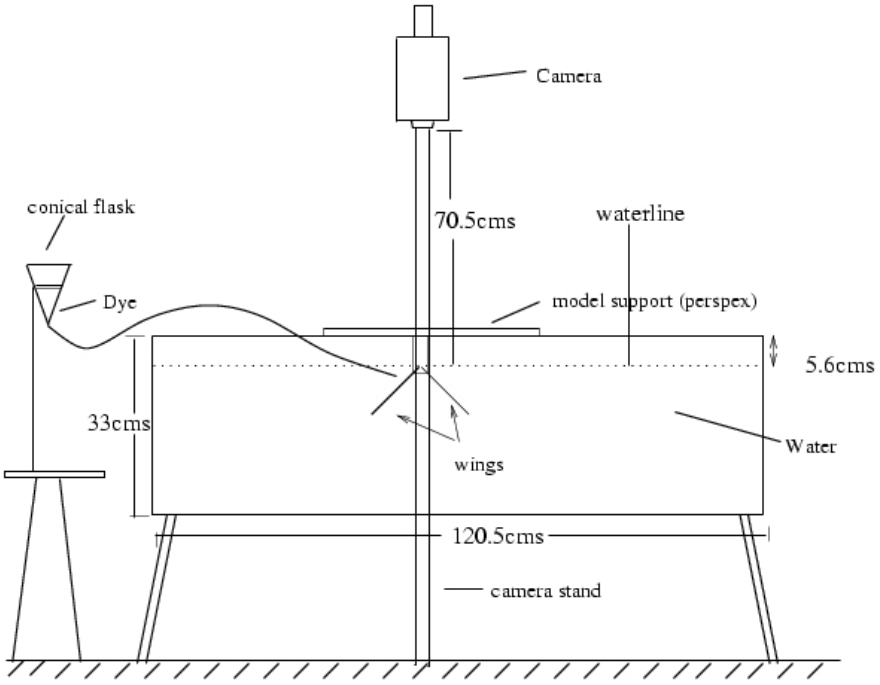

Fig 2.9 Diagrammatic representation of the flow visualization setup (front view)

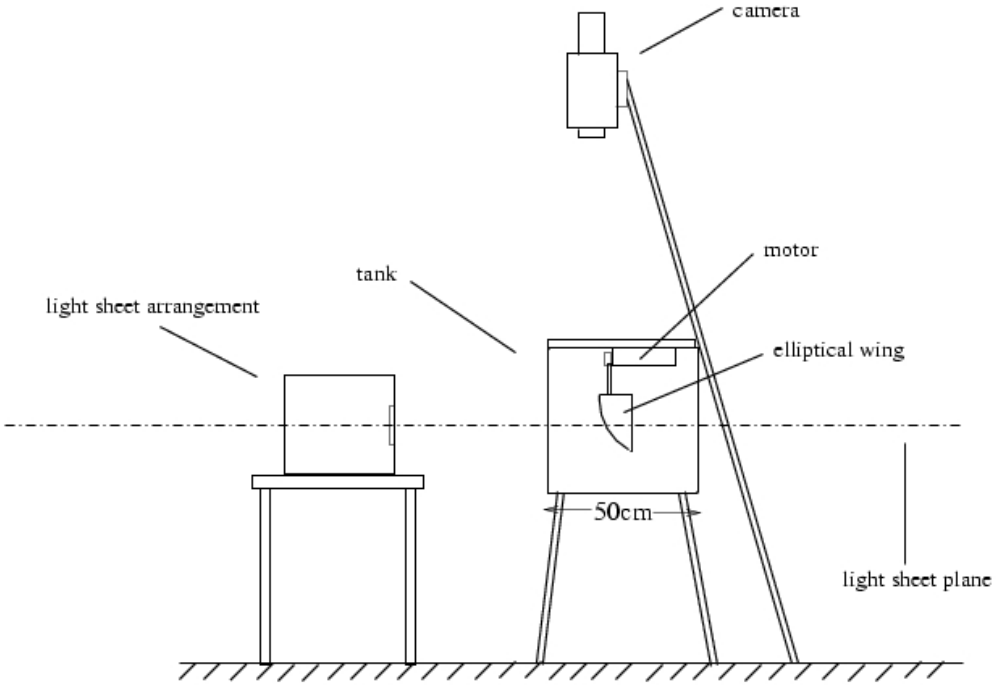

Fig 2.10 Diagrammatic representation of the flow visualization setup (side view)

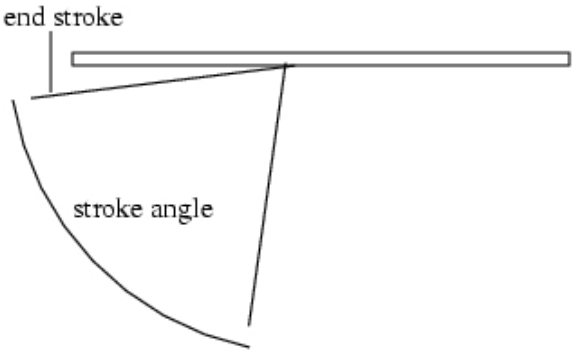

Fig 2.11 Stroke angle of the wing (front view)

The frequency of flapping at which experiments were performed are 0.46Hz and 0.7Hz for single wing model, and 0.2Hz for double wing model. The models were placed upside down such that the motor can be kept outside the water level. A light sheet was used to illuminate a particular plane and flow field was visualized using a camera perpendicular to this plane.

3. Results and Discussion

PIV results

Experimental results obtained from measured velocity and vorticity field using PIV are presented in this section. Analysis and comparisons are made for each stroke positions for the 1X and 1.75X wings of model 1. The measurements are taken at 3 locations of these wings. For the 1Xmodel the measurements are carried out at 0.5R, 0.7R and 0.8R from the root of the wing, where R is the span of one wing (Fig2.1). For the 1.75X wing measurements are done at 0.4R, 0.6R and 0.7R from the root of the wing. The sequence of flow visualization images, velocity and vorticity field data is presented at 0.4R spanwise location for 1.75X wing sizes (Fig3.1). The velocity and vorticity levels are shown adjacent to the corresponding PIV images. The results of both the wings are compared to understand the variation of flow properties with frequency and wing size. The flapping frequency is kept constant for a wing during measurements (4Hz for 1.75X wing, 6Hz for 1X wing). The mechanisms and the typical flowfield are discussed in details for one sequence

Flow field of 1.75X wing at 0.4R spanwise distance from root in model 1 is shown in Fig 3.1. Fig 3.1 a shows the flow field from t = 45ms (milliseconds), where t = 0 is the time when the wing is at the beginning of downstroke. Even at this time when the downstroke has just started the trailing edge vortex (TEV) that wraps around the wing is observed. The effects of the last upstroke suction are also observed in Fig 3.1a. These vortices as seen are the results of the last upstroke the details of which shall be discussed in the upstroke part. These vortices still present in the downstroke are quite weak in strength and fades out quickly as downstroke progresses. In this picture the leading edge vortex (LEV) is not seen due to absence of any seeding particle near leading edge. The LEV is seen in Fig 3.1b, which also starts forming with the TEV a little after the start of the downstroke and increases in strength as the stoke progresses. This is observed in Fig 3.1a-i and inferred from the values of vorticity field as well as the size of the LEV. The blue color shows the LEV as clockwise (negative vorticity values) as from the direction the wing is seen the leading edge is on the left side. Similarly the TEV is in red and yellow color as the circulation is anticlockwise (positive values). The growth and evolution of LEV and TEV is clearly seen in 3.1a-i. This attached LEV is believed to be one of the important factors in the lift production in flapping flight and even at higher angle of attack as it delays the stall (Dickinson et al, 2001). As there is no forward velocity in the experiments performed, the LEV and the TEV are connected and forms a single structure which runs over the whole periphery of the wing. The vorticity levels of LEV and TEV can be seen to be equal and opposite at all positions of the downstroke and even at different locations in accordance with Kelvin's conservation of circulation. This low pressure zone over the wing produces a high lift and a little thrust depending upon the orientation of the wing at that point of the stroke. The downward velocity above the wing (between LEV and TEV) increases as the wing moves down (see Fig 3.1a-c). There is always a downstream velocity present even though these experiments are at zero advance-ratio. The flow is unsteady being in the wake of LEV and probably is responsible for the instability of TEV, which is observed to be broken down in tiny shear

layer vortices as time progresses (Fig 3.1 b to d). The high velocity fluid (downward) creates a suction to engulf a part of the TEV and forms a recirculating zone as shown in Fig 3.1d. The LEV grows with time, reaches its maximum strength as the stroke progresses in Fig 3.1h and starts to fall in strength at the end of the stroke as the reversal of stroke begins to start in Fig 3.1i.

As the stroke changes from downstroke to upstroke, due to the opposite motion of the wing another tiny vortex develops below the wing as shown in Fig 3.1j. This vortex (which is of opposite circulation to that of the TEV) is small in size and strength, as compared to the TEV at this point of the stroke. The TEV interacts with this vortex (Fig 3.1j) and both being closer to each other, the induced velocities on each other is high. As a result both the vortex pair is ejected at a very high velocity along the trailing edge satisfying the Kutta condition (see Fig 3.1k). Even before ejection of these vortices pair due to there mutual interaction, the fluid in between these two vortices gains momentum due to the induced velocity. Because of the ejection of fluid as a jet and the vortices as a pair, a high momentum is in turn imparted to the wing as per the momentum conservation. This results in a high amount of force in the opposite direction of the ejection, on the wing. This ejection moving downwards in well visualized in Fig 3.1k-o.

Apart from this ejection phenomenon, there is a collapse of the earlier LEV and TEV pair which initiates with the stroke reversal as shown in Fig 3.1j-k. These two vortices which were connected in the downstroke, during the beginning of upstroke start to collapse due to their self induced velocity (the shape being non-circular). The effect of this collapse on the wing or on force generation is not fully understood yet.

As the upstroke progresses the vortices of opposite circulation to the earlier LEV and TEV pair grow below the wing (Fig 3.1k-m) thus, creating a downward force on the wing but an increase in the subsequent thrust generation due to the feathering resulting in momentum transfer at an angle which resolves finally to downward force and thrust in two perpendicular directions. After the ejection along with the jet, the vortex pair (Fig 3.1k) doesn't vanish downstream rather is reutilized in the suction due to upstroke in Fig 3.1o-r. This phenomenon is termed as wake capture and it is well observed that the pair of vortices just shed away at the stroke reversal at early of upstroke is reutilized in the suction of the wing in absence of any forward velocity. In case of non-zero advance ratio the same phenomenon is observed with varying strength if the advance ratio, $J < 1$ and flapping frequency is high. Thus the wake capture is possible if the stroke reversal is faster than the speed at which the ejection occurs. It is conjectured that the same mechanism may be used by the insects in their advantage for maneuvering.

The opposite nature vortices at the bottom of the wing during upstroke also show similar nature of growth like that of LEV (Note that LEV is defined as the vortex formed at leading edge during downstroke only) but its strength is comparatively lower than LEV (Fig 3.1j-r). This explains that the positive lift in downstroke is more than the negative lift created in the upstroke due to these opposite vortices. Thus there is a net lift in the whole cycle.

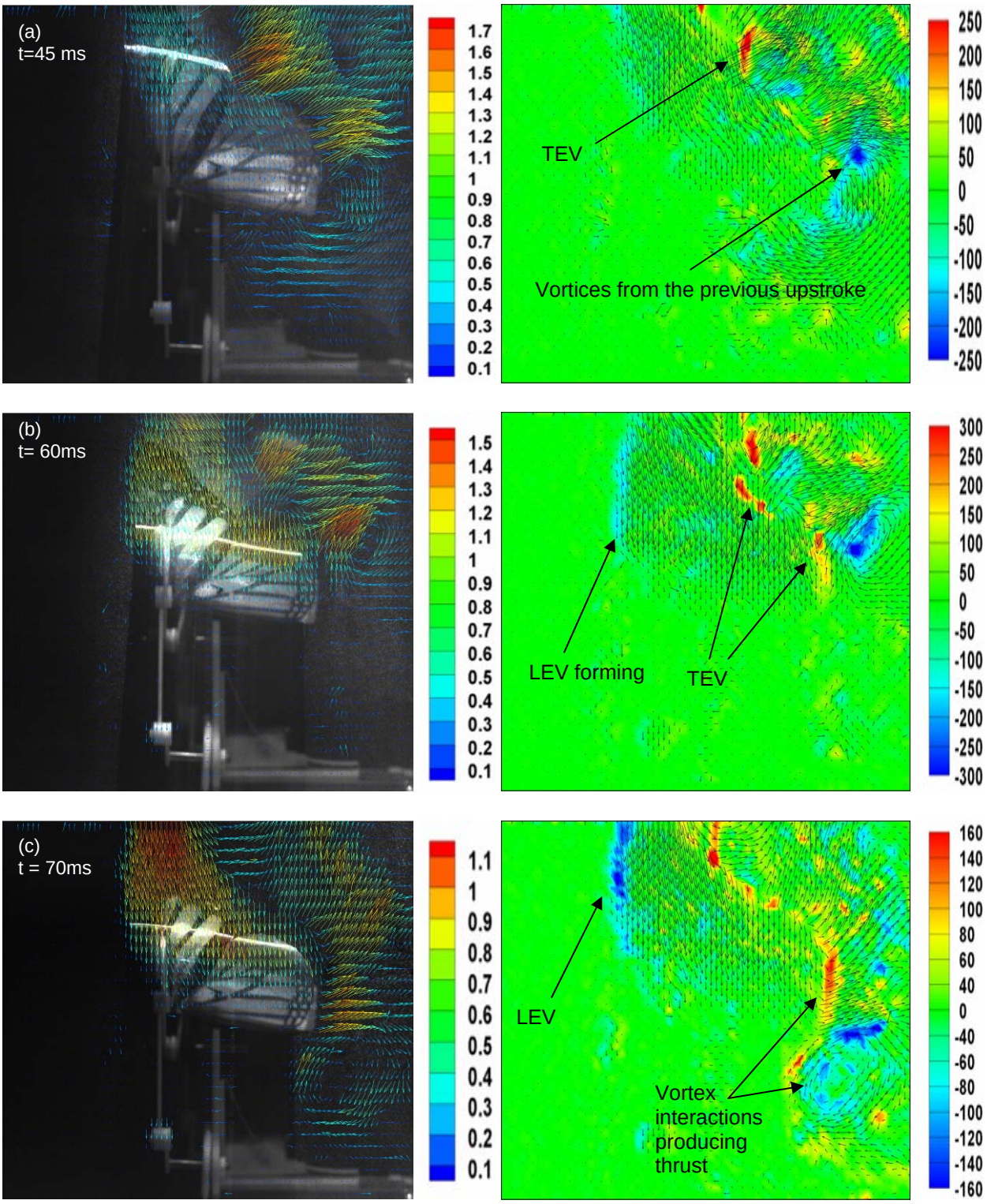

Figure 3.1 (a), (b), (c). Downstroke: beginning, formation of LEV, vortex interactions with the previous stroke producing thrust (for 1.75X wing at 0.4R at 4Hz); velocity and vorticity fields.

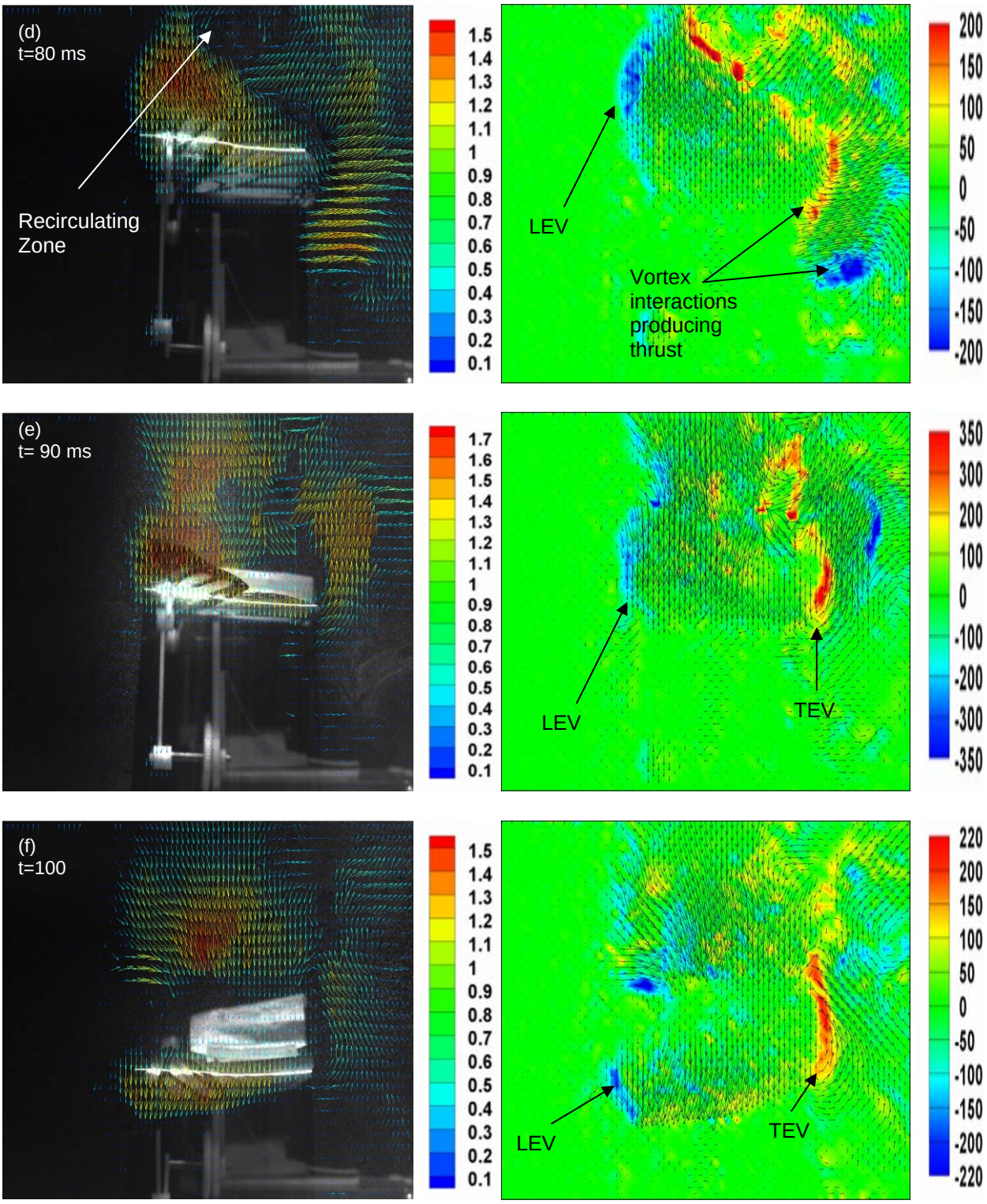

Figure 3.1 (d), (e), (f). Downstroke: growth of LEV and TEV (for 1.75X wing at 0.4R at 4Hz); velocity and vorticity fields.

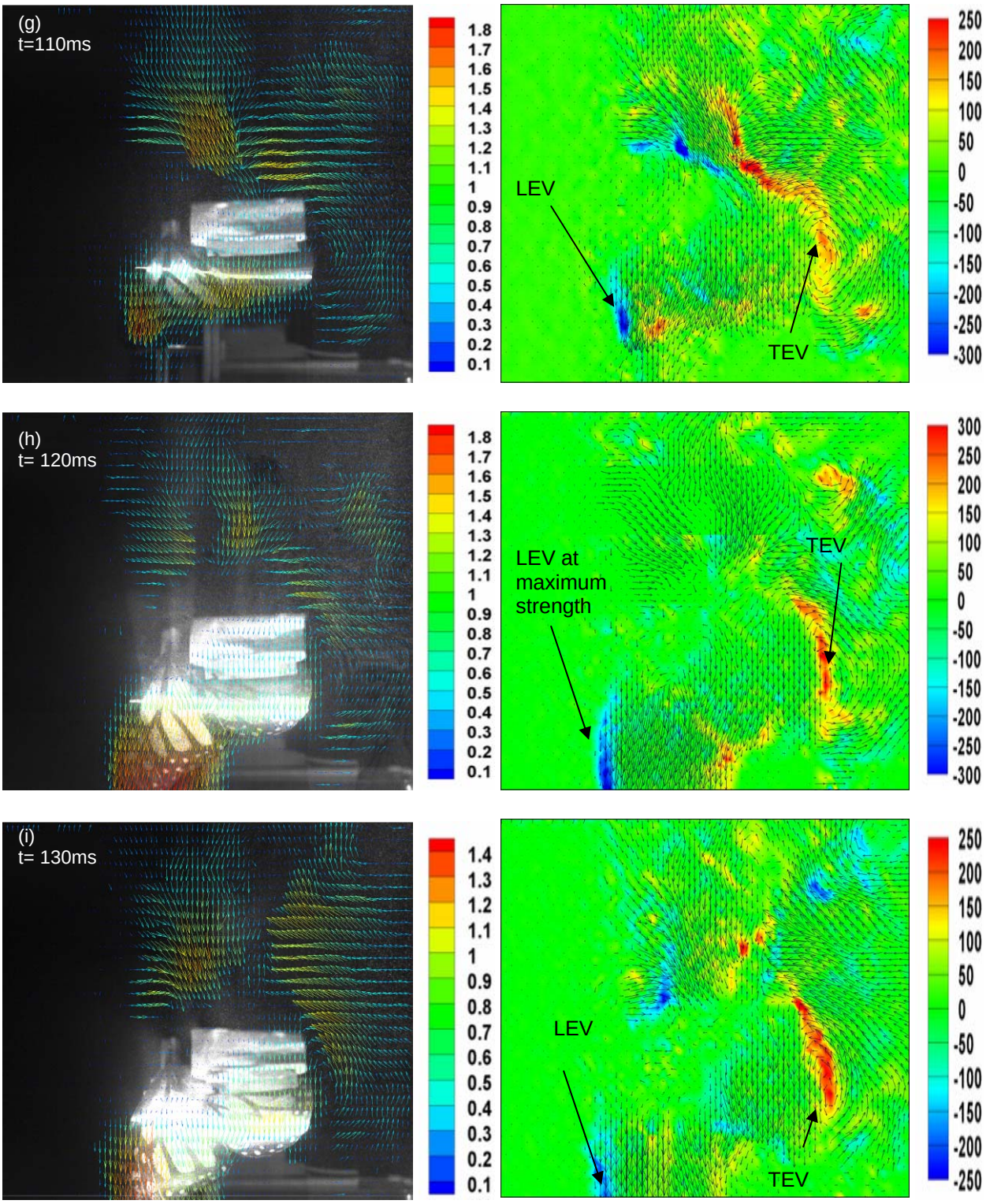

Figure 3.1 (g), (h), (i). Downstroke: LEV and TEV maximum towards the end (for 1.75X wing at 0.4R at 4Hz); velocity and vorticity fields.

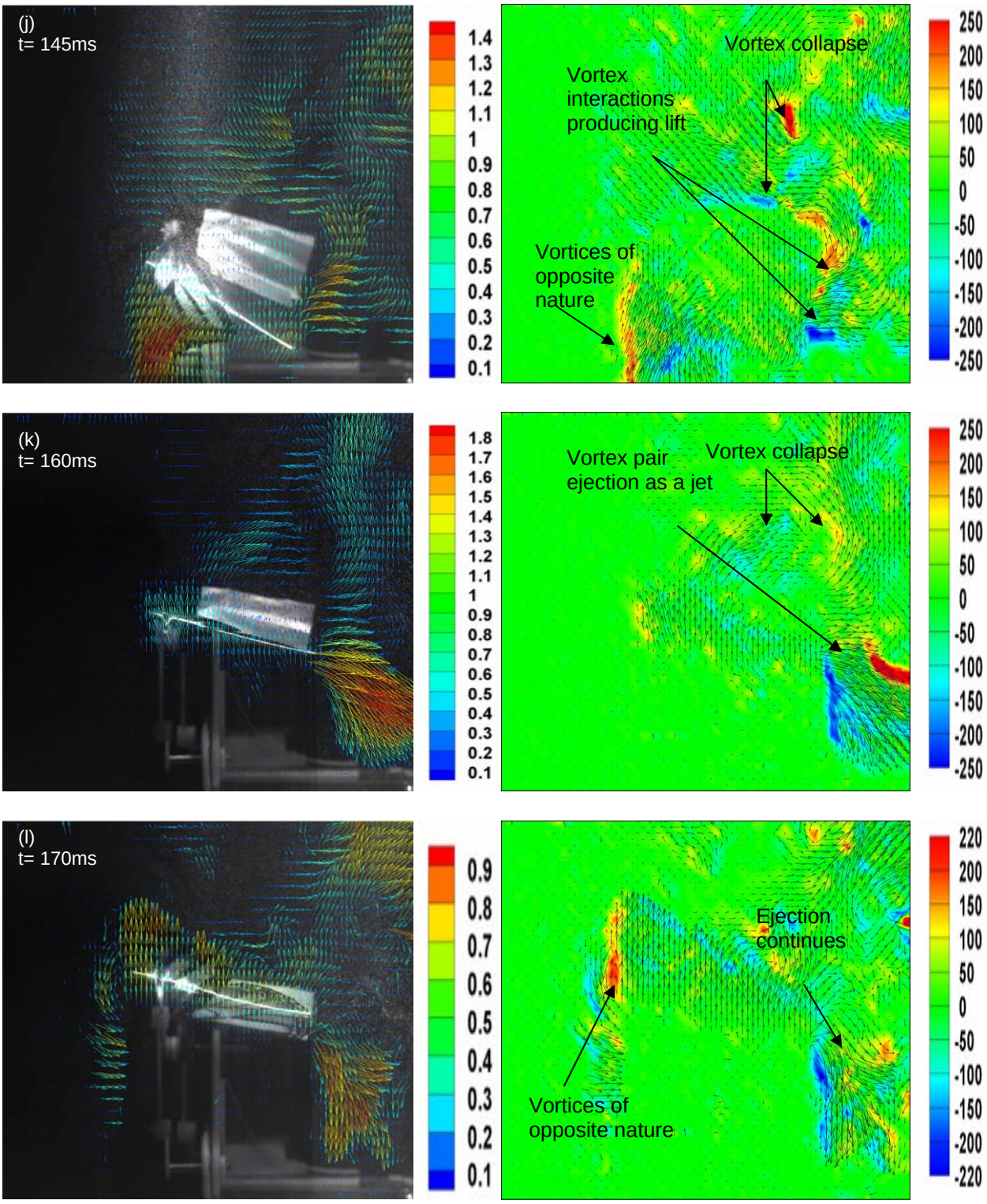

Figure 3.1 (j), (k), (l). Upstroke: beginning, vortex interaction, ejection of vortex pair (for 1.75X wing at 0.4R at 4Hz); velocity and vorticity fields.

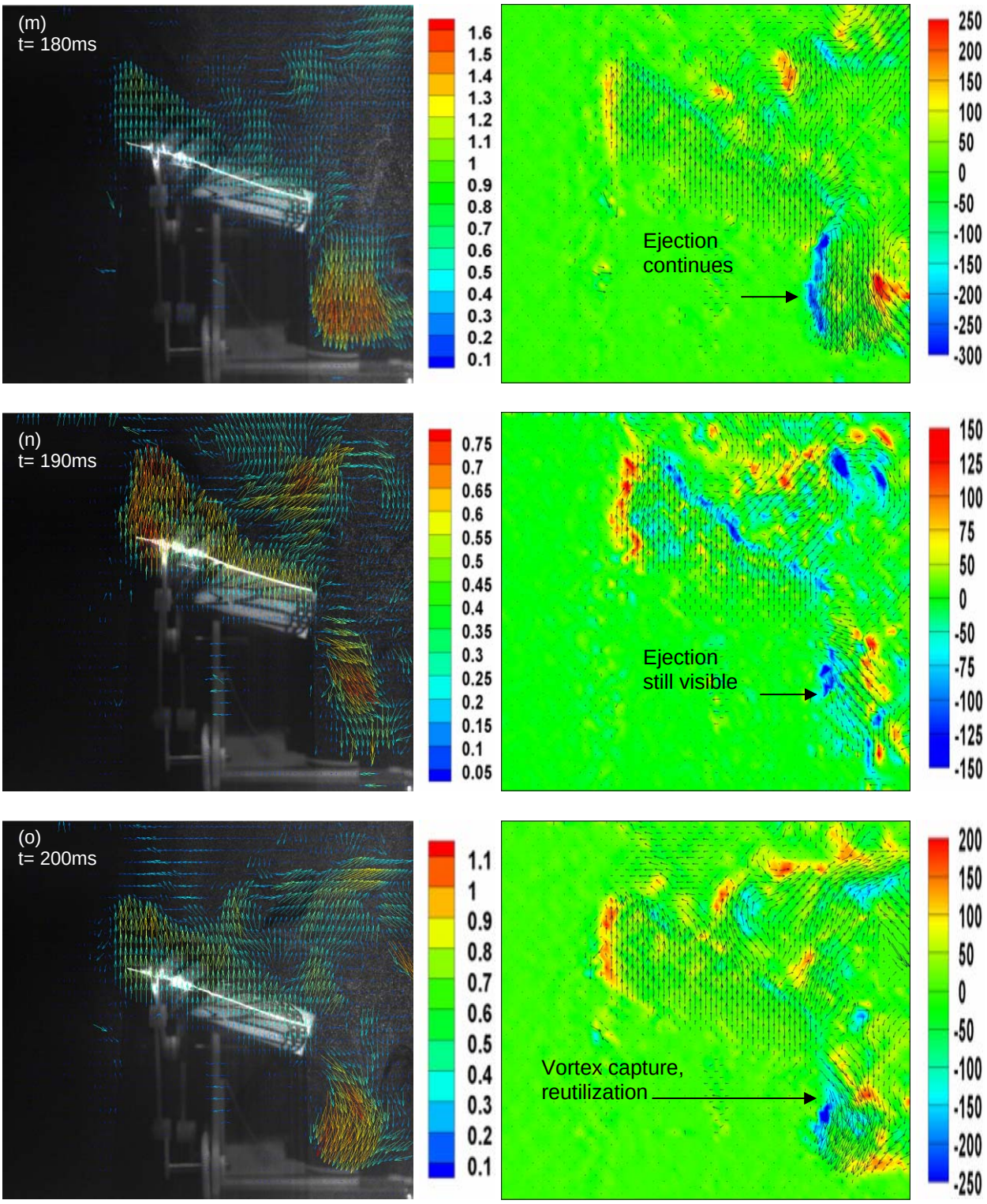

Figure 3.1 (m), (n), (o). Upstroke: shedding continue, wake capture (for 1.75X wing at 0.4R at 4Hz); velocity and vorticity fields.

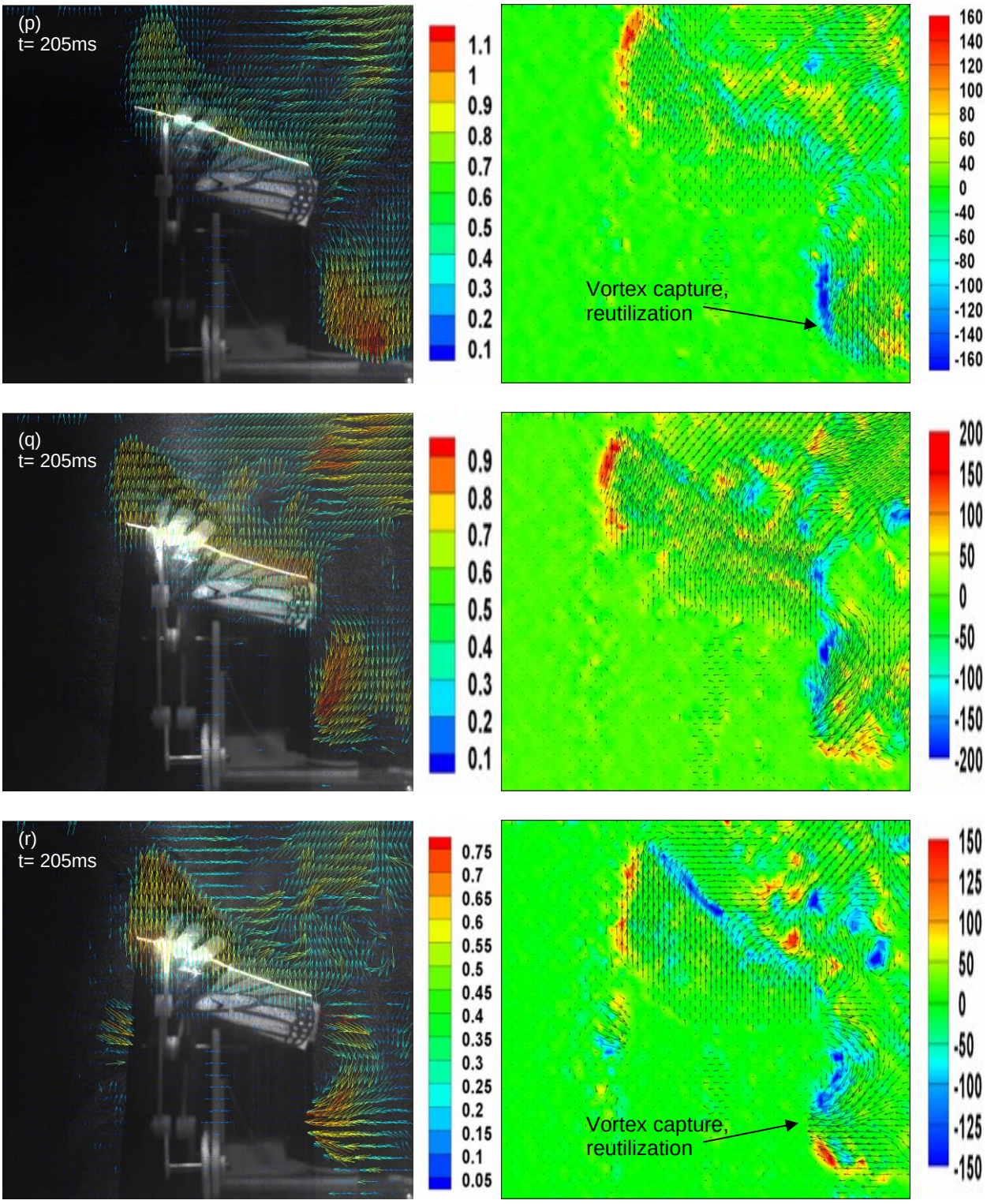

Figure 3.1 (p), (q), (r). Upstroke: wake capture continues, vortices are reutilized (for 1.75X wing at 0.4R at 4Hz); velocity and vorticity fields.

As upstroke finishes and downstroke starts there is another vortex interaction as seen in Fig 3.1a. With the advent of the next downstroke again, the TEV starts forming with LEV. This newly formed TEV interacts with the already existing vortex in the upstroke. Hence there is another ejection just like the one before, but this time it adds more to the thrust as the feathering angle is very horizontal. The nature of the shedding at both stroke reversals is similar, but the amount of this force generated out of it to lift and thrust is not same in both the times. It can be seen from Fig 3.1k that the angle of ejection is more towards vertical so it will add up to lift more. Whereas in Fig 3.1a the angle of ejection is more towards horizontal thus adds up to thrust more. Thus, the insects utilize the vortex interactions by varying the feathering angle during stroke reversals.

The general mechanisms of LEV formation, its growth, its decay in the downstroke, the jet ejection or shedding at the stroke reversal owing to the vortex interactions, the LEV TEV collapsing, vortices growing of the opposite nature in the upstroke, the subsequent vortex capture and finally another shedding and vortex interaction at the start of downstroke is well observed in Fig 3.1. These general observations are quite similar for the other sequences as well at different spanwise location and different wings. Only the strength of the vortices at different spanwise location becomes the function of the sectional Reynolds number, other physics and flowfield being the same.

The variation of maximum vorticity with time for the LEV is plotted in Fig 3.2, 3.3 with the corresponding time of the stroke for each measurement presented here. The strength of this vortex is growing with time as inferred from the size of it seen in Fig 3.1. The force generation and its nature due to this LEV growth and evolution are in agreement with the ones estimated in the literature (Ellington, 1996, 1999). The forces generated in the downstroke are largely contributed by this LEV for insects whereas in birds a part of the lift and drag is produced due to the airfoil shape of their wings.It has been observed that there is a significant difference in the strength of the vortices produced and timings of the key events described above. Firstly, there is a change in the strength of LEV along different locations for both wings. The LEV grows in size and strength towards the tip of the wing. This nature is observed for both the 1X and 1.75X wing. Hence for the same wing and for the same flapping frequency, the strength of the LEV varies along the length of the wing, its strength is very low at the root of the wing and it’s maximum at the tip of the wing. This variation can be seen at different spanwise locations in our experiments in Fig 3.2 for 1.75X wings. This observation justifies the notion of LEV of class III (Ellington, 1996). Various categories of LEV are already mentioned in the first chapter. Thus this type of LEV is an individual structure present over each wing and the strength of which increases along the span of the wing towards the tip.

It is concluded from the PIV results that the strength of this LEV depends on local Reynolds number (Re) based on the tip velocity and chord length of a particular cross section of any wing over which the measurements are taken. This is because in spite of the difference in flapping frequency of both the wings the strength of LEV is quite similar at same Re. In Fig 3.2 & 3.3 the LEV strength of 1.75X wing is little more as the tip velocity is slightly greater for bigger wing ($U=2\Phi Rf$). The Strength of the LEV is also a function of J. With wing stiffness and flexibility coming into play for small flying

insects, the nature of this LEV becomes dependent on them, though it has not been shown quantitatively. As the experiments here are done with no forward velocity of wind, the strength will only be depending on the wing flexibility and flapping velocity. We have used a single material for the wing (Mylar membrane) so the effects of flexibility or rigidity can't be shown. With no forward velocity the effects of unsteady nature can be better studied, whereas with higher forward velocity the consideration goes to the quasi steady regime. Flapping velocity depends on frequency of flapping and the distance of the section from the root of the wing ($U=2\Phi Rf$). So with higher frequencies of flapping or with higher span length of the wing, the LEV grows stronger along with Re.

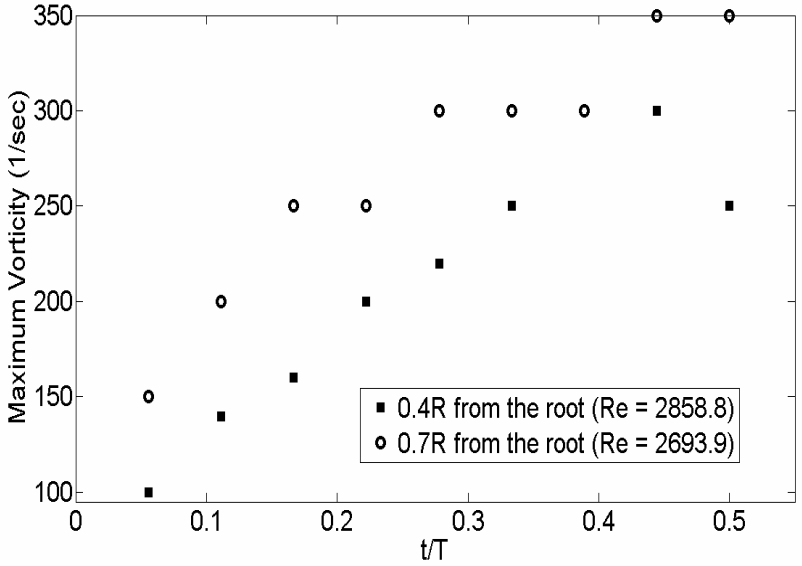

Figure 3.2 Variation of maximum vorticity of LEV with time at two locations for 1.75X wing

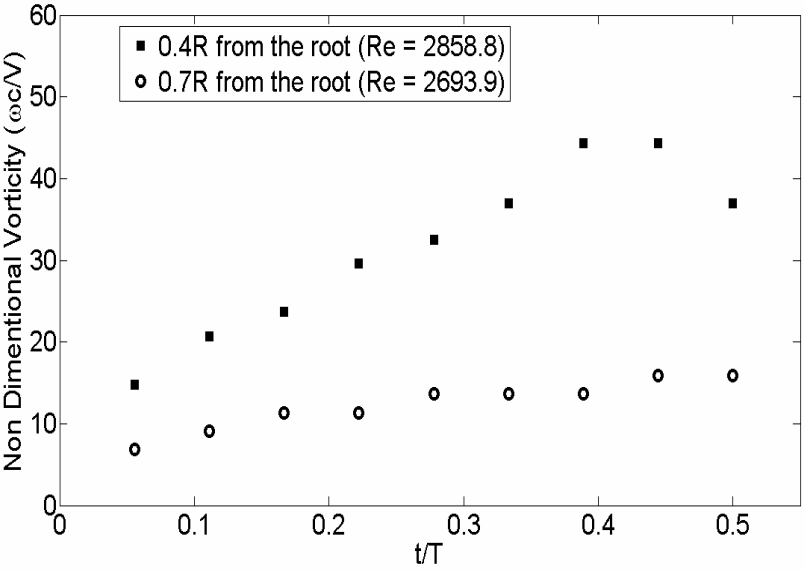

Figure 3.3 Variation of maximum vorticity of LEV with time at two locations for 1X wing

Force results

Model 1 results

The data from load cell experiments are in terms of voltage and contained significant higher frequency noise at low flapping frequencies. The noise is eliminated using filters. Voltage data is converted to force using appropriate calibration of load cell. For the latter purpose the calibration is done by loading the set up by dead weights of 100gm, 200gm and 300gm without flapping and noting down the output voltage through the amplifier for the insect model. The change in voltage with each 100gms of weight came out to be same, so the force vs voltage graph is a straight line. The slope of this curve is 230.6863gm/volts which is the calibration coefficient. To remove the higher frequency noise a low pass filter is used in Matlab to filter out any frequency over 25 Hz. The flapping frequency is calculated by taking the FFT (fast Fourier transform) of this filtered data which is seen as a major peak in the plot (Fig 3.4d). This frequency is cross checked by the visualization using PIV. The cross checking is basically done to add to more certainty to the output data. Fig 3.4 shows the processing of the data in steps. Fig 3.4a shows the raw data for 1X wing when supplied with 8V to the dc motor (Flapping frequency = 12.3Hz). After filtering the noise (> 25 Hz) the data is Shown in Fig 3.4b. After shifting the scale to zero and multiplying with the calibration coefficient the data is shown in Fig 3.4c. An enlarged view of the same can be seen in Fig 3.4d. The flapping frequency of the raw data of about 12.3Hz can be clearly seen from the peak in the FFT curve in Fig 3.4e where another peak is at 50Hz (noise). The flapping is started a few seconds after the data has already started being recorded. This can be seen from a low band and then the high fluctuations over it as the flapping starts.

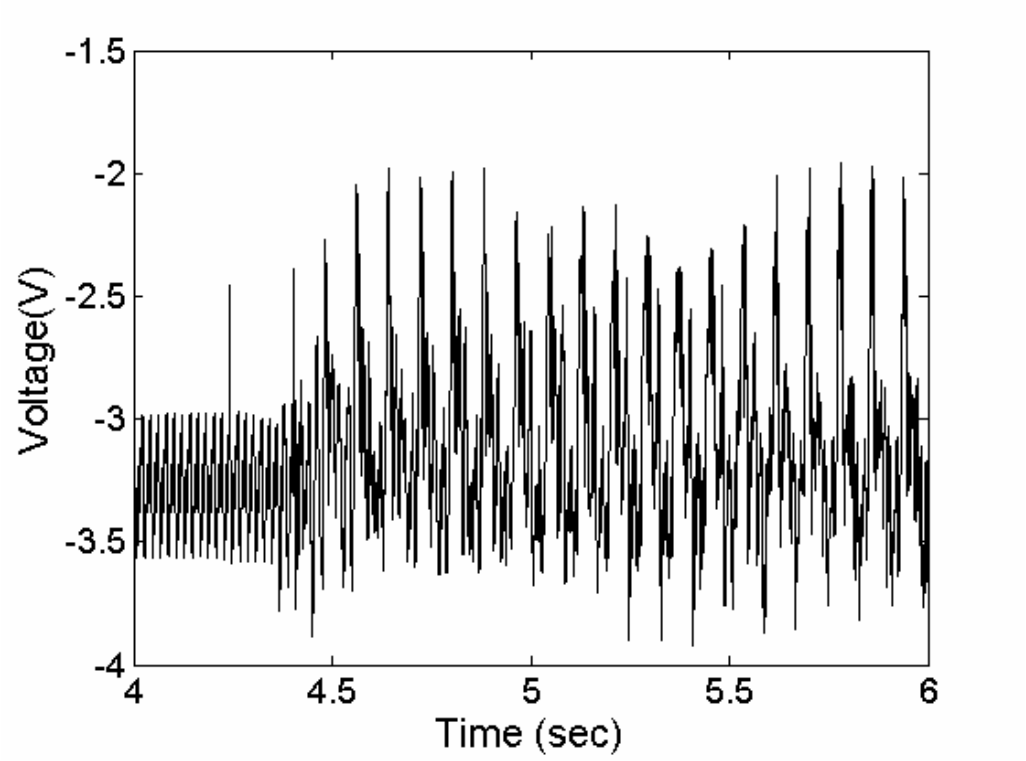

Figure 3.4 (a). Raw Data from the load cell for 1X wing (Model 1) at 12.3 Hz

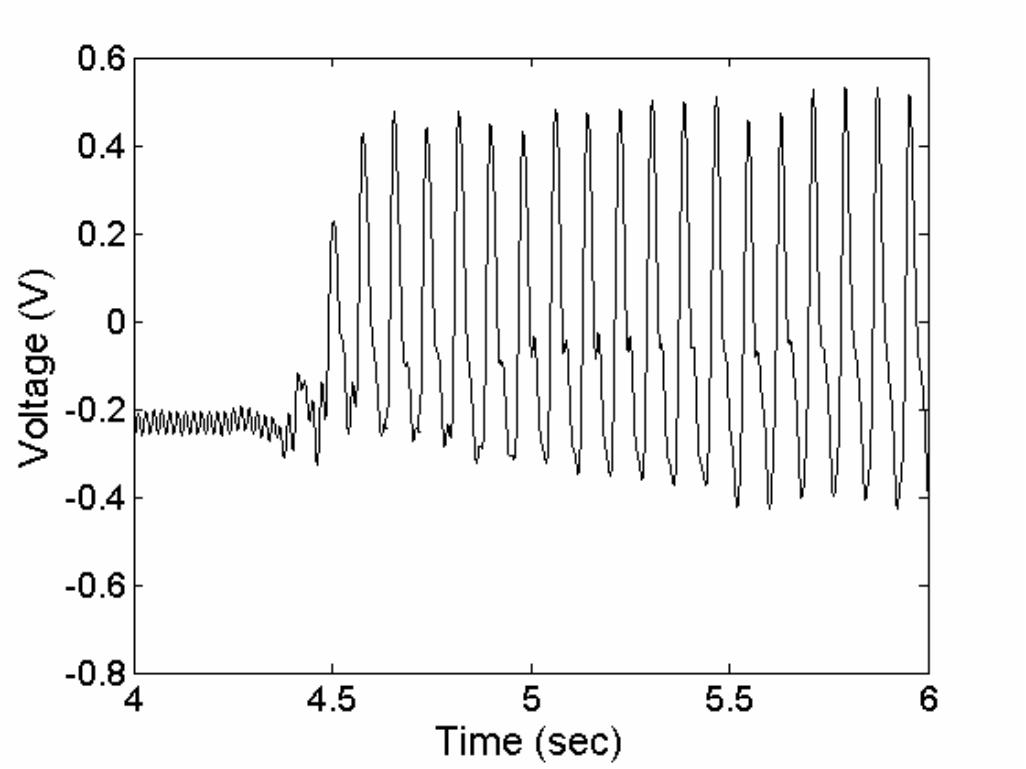

Figure 3.4 (b). Data after filtering frequencies over 25 Hz

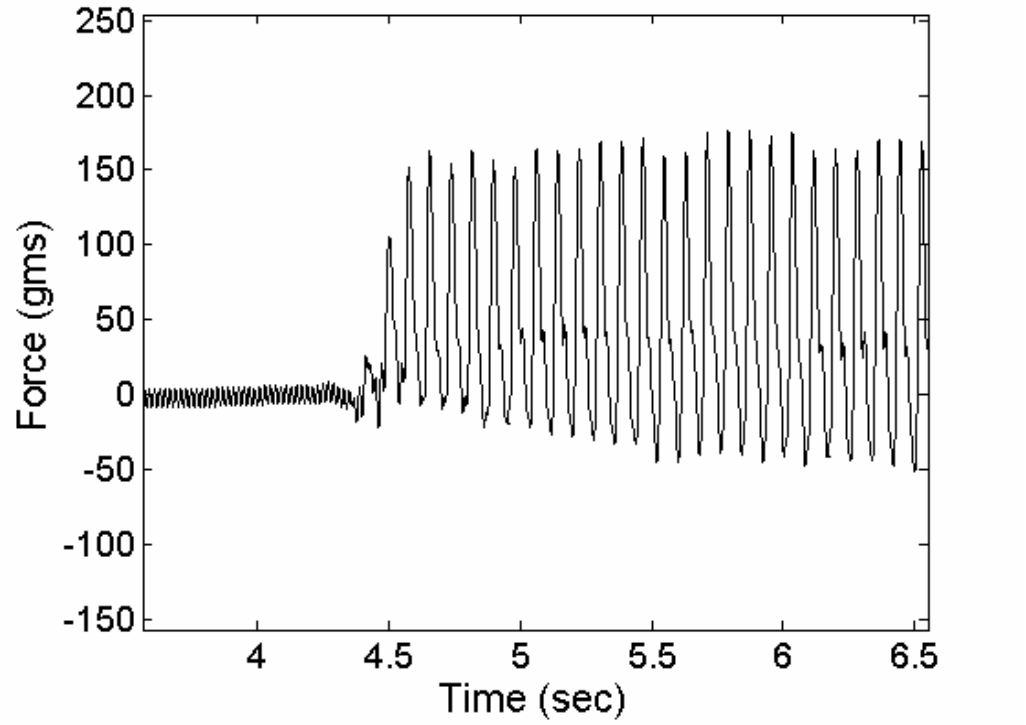

Figure 3.4 (c). Lift Vs Time data after multiplying filtered data by calibration coefficient and shifting it to zero level.

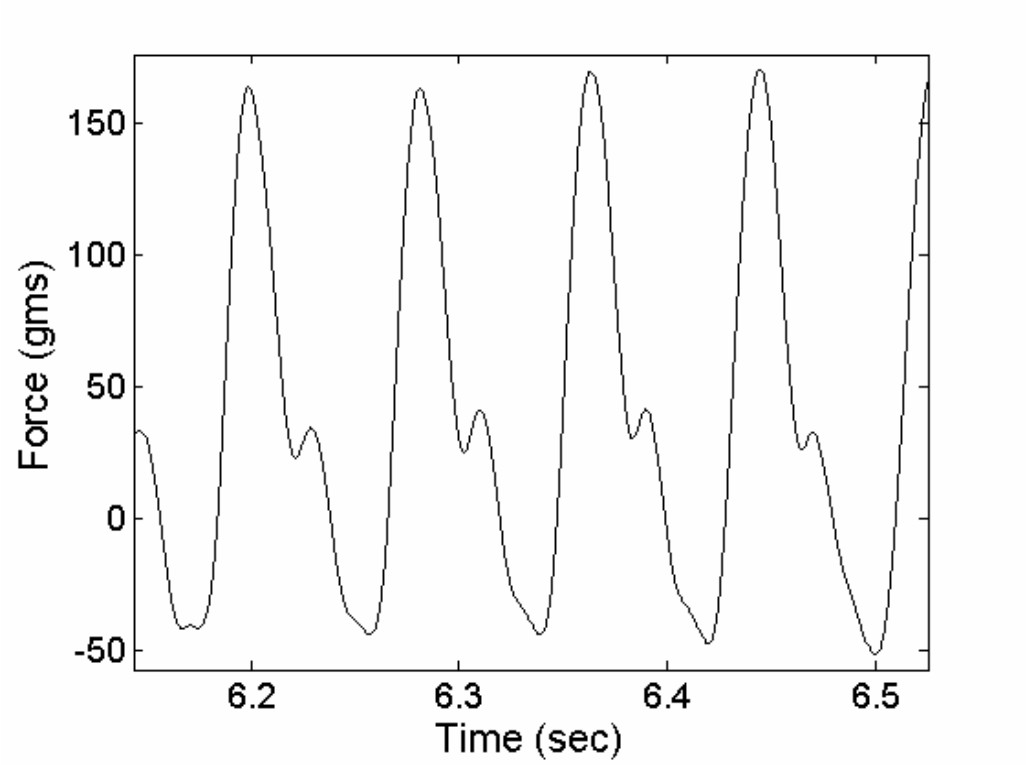

Figure 3.4(d). Zoomed view of the data of Fig 3.3(c)

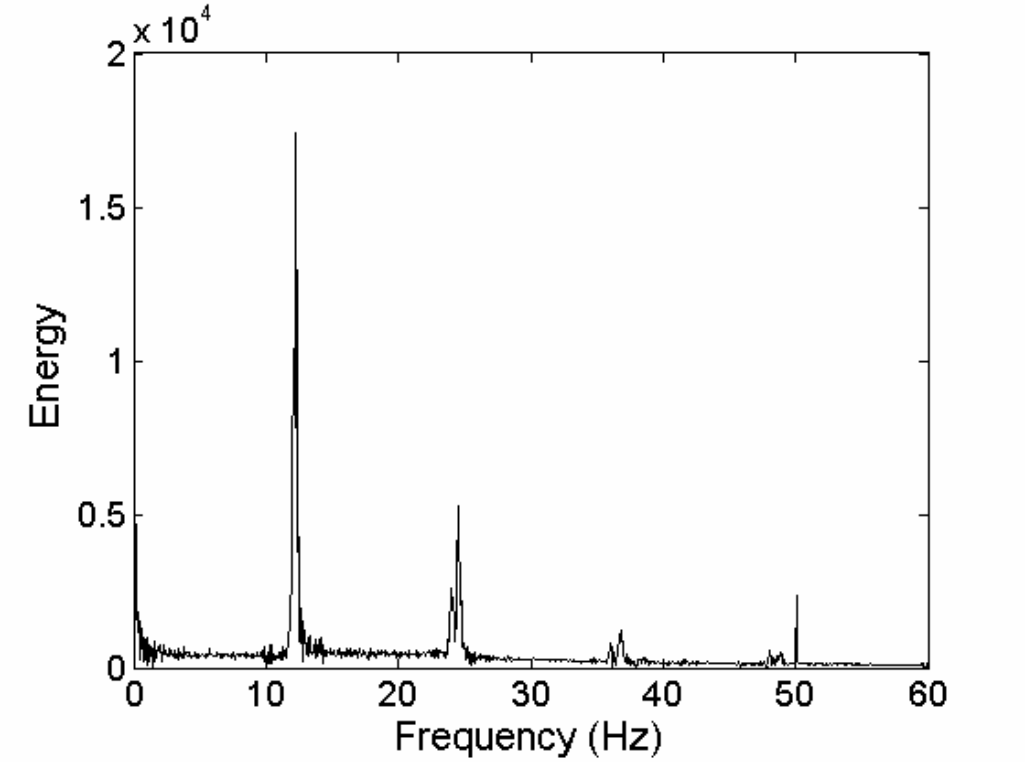

Figure 3.4 (e) FFT of the filtered data, peak of 12.3 Hz clearly seen.

Similarly, we did the same for all the experiments carried out on all the 3wings on various flapping frequencies. Then the average lift, maximum lift, minimum lift, average drag and net drag are calculated from these plots. All such data is tabulated for all the wings in Table 3.1, 3.2 and 3.3.

Frequency (Hz)	Lavg (gms)	Lmax (gms)	Lmin (gms)	Tavg (gms)	Tnet (gms)
12.30	22.82	165.17	-68.18	1.880	24.49
11.75	9.92	122.96	-50.38	1.530	19.94
11.40	9.60	117.75	-48.27	1.730	17.43
11.10	9.45	116.94	-47.02	1.300	14.08
10.70	9.22	111.13	-45.72	0.990	10.22
9.25	10.15	107.06	-43.41	0.900	10.60
9.05	8.34	95.07	-41.27	0.810	10.65
8.45	5.21	71.41	-30.89	0.670	12.93
8.05	3.81	49.57	-24.03	0.667	15.53
7.30	4.52	67.63	-26.67	-0.600	4.97
6.6	3.43	43.51	-25.81	-0.840	2.50

Table 3.1 Lift and thrust data for 1X wing (model 1)

Frequency (Hz)	Lavg (gms)	Lmax (gms)	Lmin (gms)	Davg (gms)	Dnet (gms)
5.90	3.477	51.455	-49.010	1.635	12.274
5.70	3.397	44.058	-42.047	1.819	12.685
5.50	2.570	40.600	-39.272	1.618	10.690
5.25	2.760	34.800	-35.930	0.998	9.950
5.05	2.638	34.110	-35.408	1.234	9.280
4.75	2.150	33.270	-36.872	1.720	10.120
4.60	-0.873	25.188	-36.680	1.540	9.175
4.40	-0.576	23.490	-35.258	0.500	3.797
4.10	-1.050	26.120	-34.570	-0.684	5.550
3.80	-1.010	22.411	-34.240	-0.708	4.877
3.35	-1.450	16.338	-29.290	-1.170	4.008

Table 3.2 Lift and thrust data for 1.5X wing (model 1)

Frequency (Hz)	Lavg (gms)	Lmax (gms)	Lmin (gms)	Davg (gms)	Dnet (gms)
5.0	3.270	42.980	-44.74	1.54	15.83
4.9	3.706	41.609	-41.72	1.74	8.83
4.8	2.890	44.850	-44.24	1.61	8.14
4.7	2.320	29.360	-32.32	1.37	8.72
4.6	2.758	29.050	-29.20	1.04	6.45

4.5	3.390	33.033	-25.65	0.55	4.93
4.3	3.218	31.690	-24.12	0.96	3.32
4.0	1.960	33.799	-24.49	0.80	3.67
3.8	1.290	23.210	-24.95	0.60	4.94
3.5	0.910	27.180	-27.37	0.33	3.5

Table 3.3 Lift and thrust data for 1.75X wing (model 1)

Finally these values of lift and drag vs frequency and the corresponding lift and drag coefficients are plotted as shown in Fig 3.5-3.10.

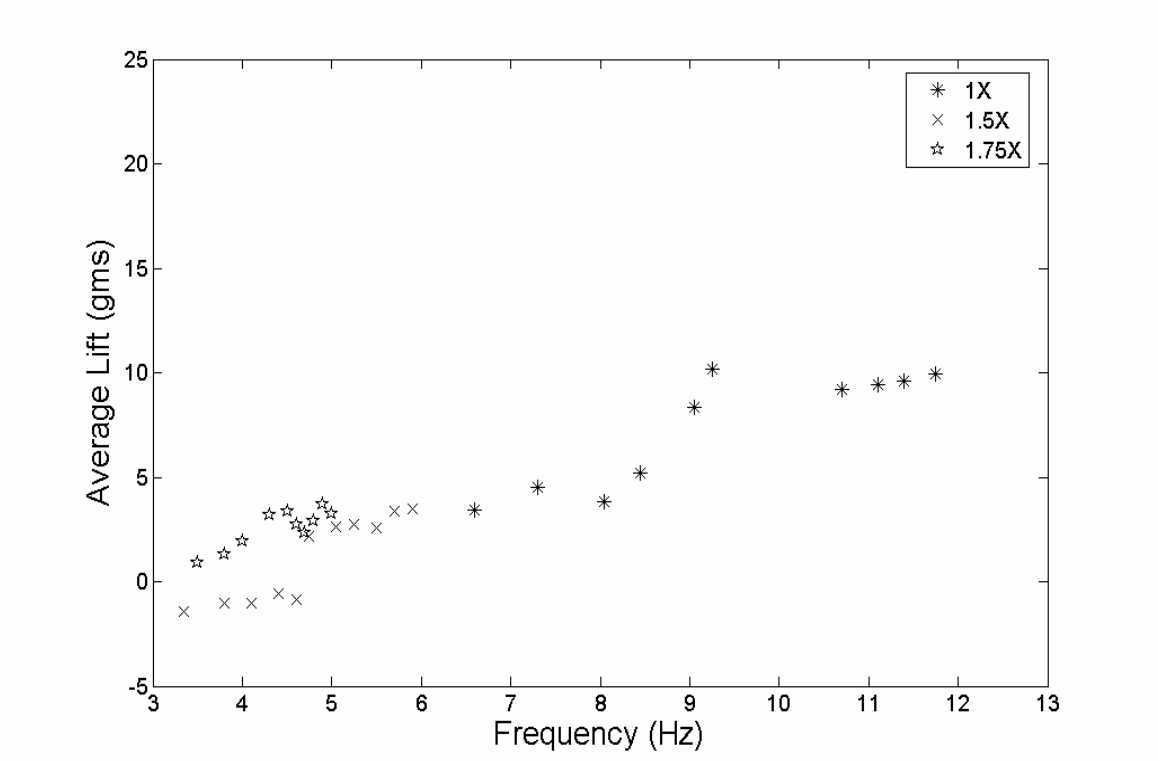

Figure 3.5 Average Lift Vs Frequency (For Model 1)

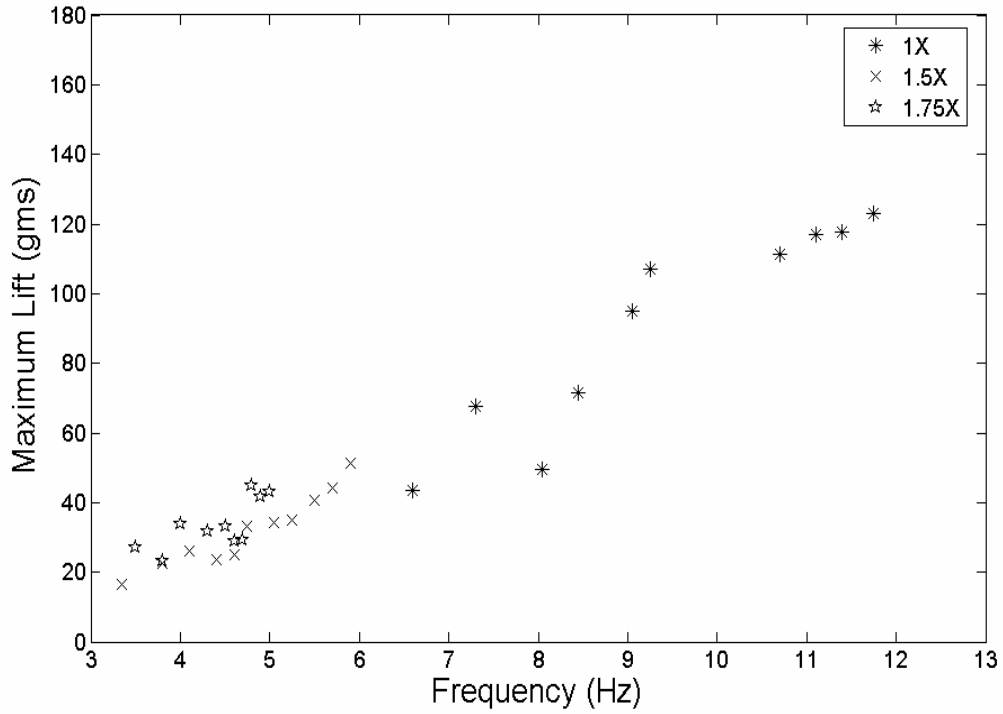

Figure 3.6 Maximum Lift Vs Frequency (For Model 1)

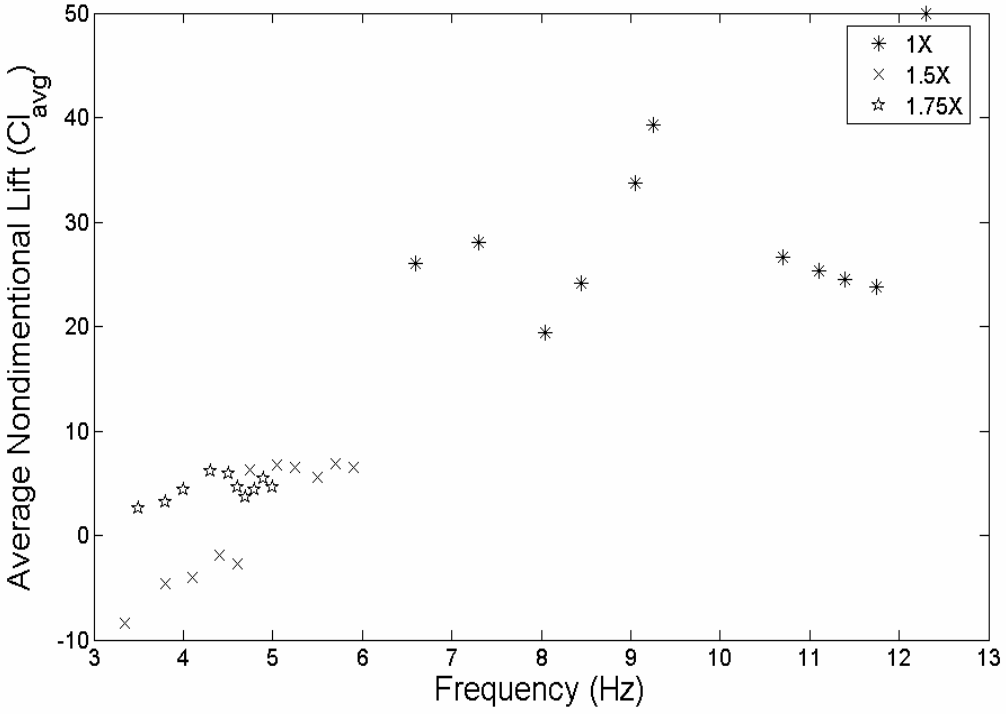

Figure 3.7 C_L avg Vs Frequency (For Model 1)

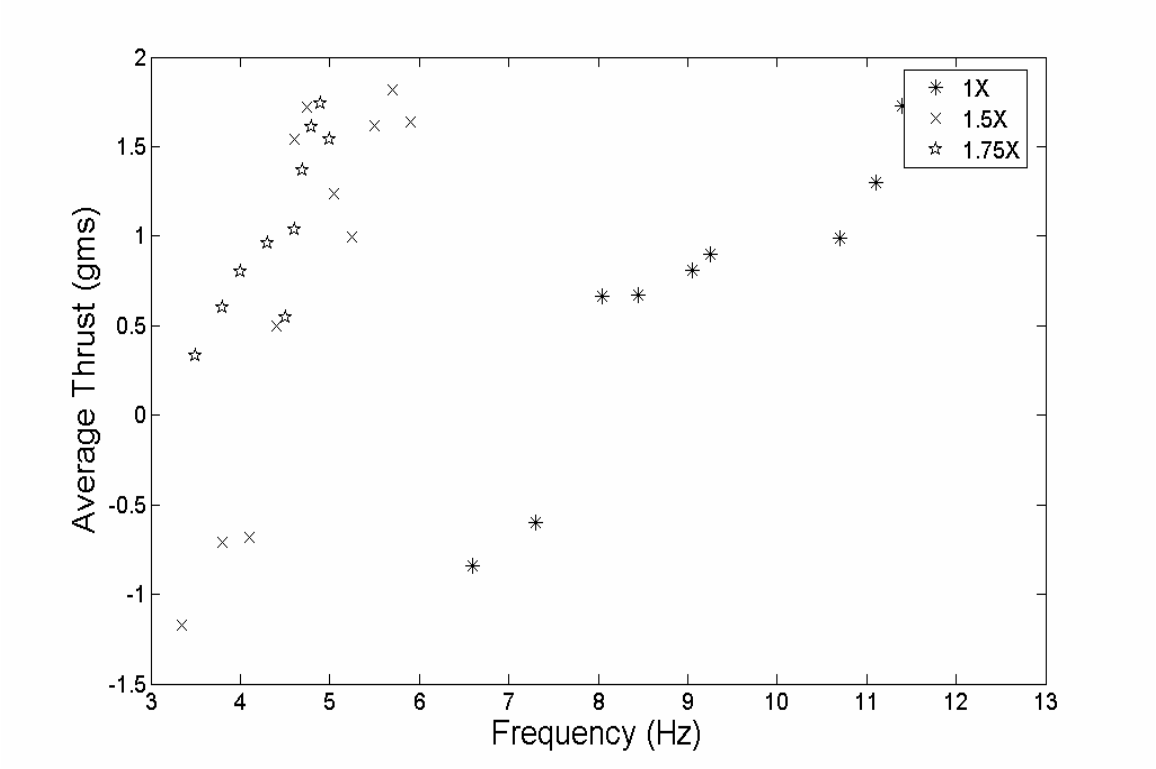

Figure 3.8 Average Thrust Vs Frequency (For Model 1)

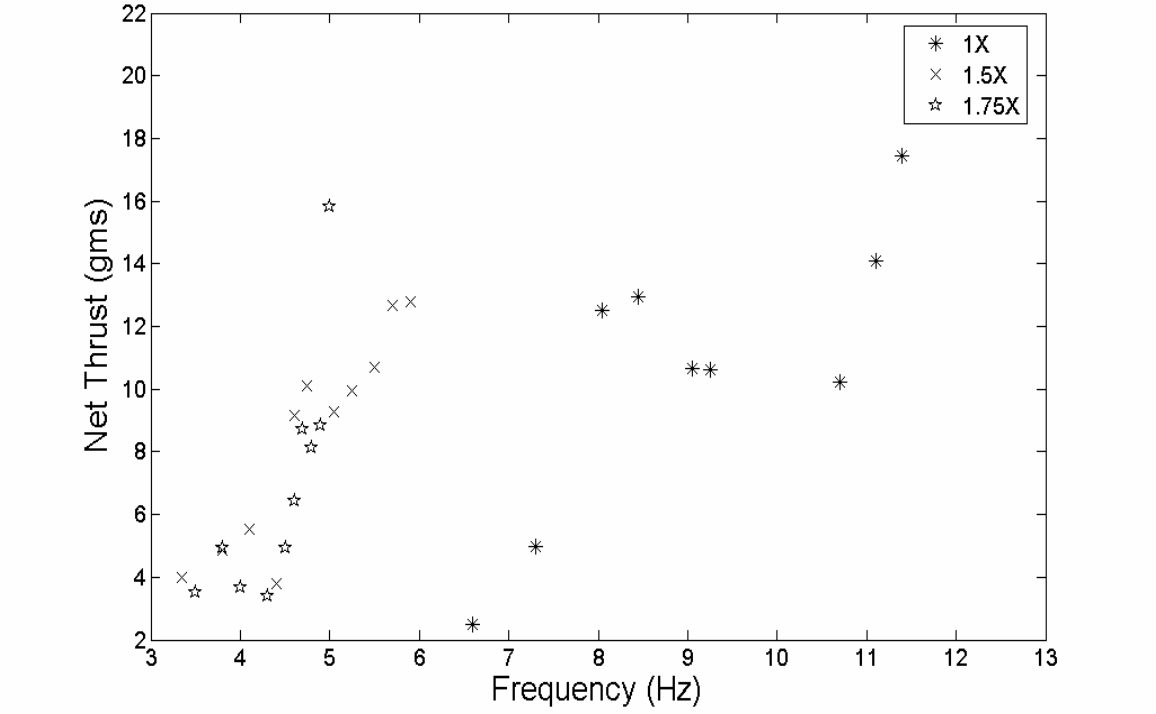

Figure 3.9 Net Thrust Vs Frequency (For Model 1)

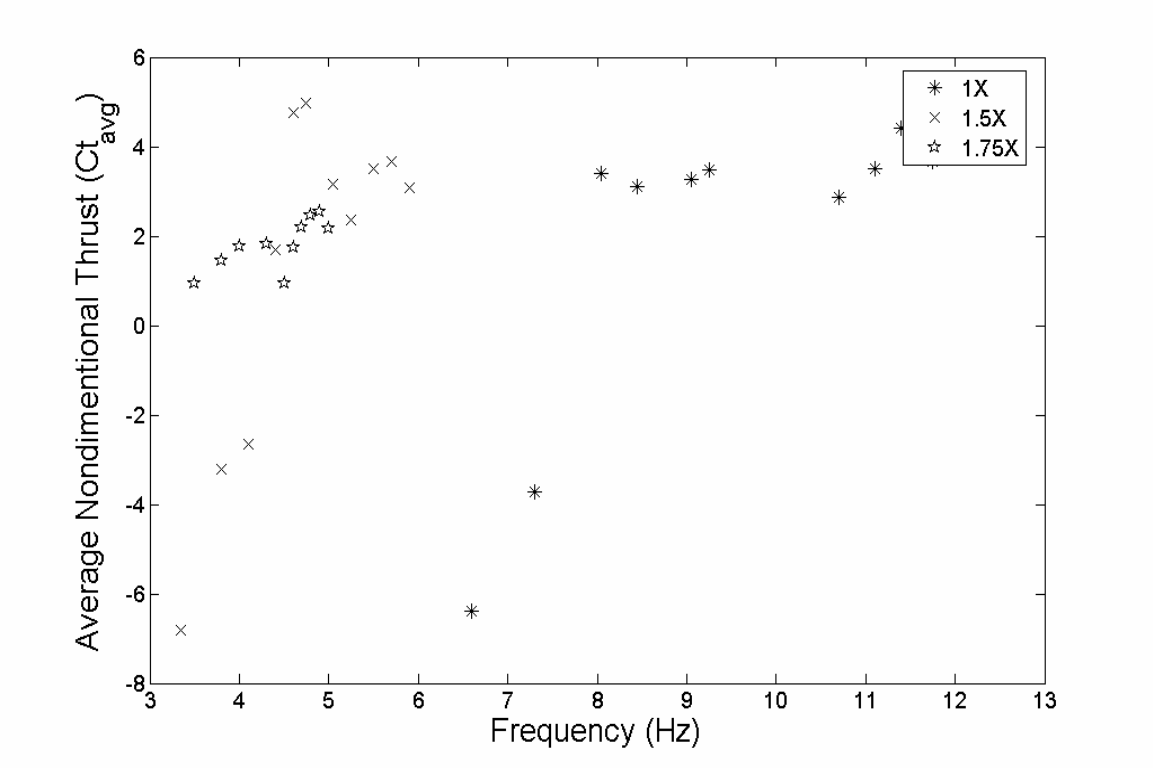

Figure 3.10 C_d avg Vs Frequency (For Model 1)

From Fig 3.5, 3.6 and 3.7 it is clear that lift is definitely a function of frequency. Though there is gap between the frequencies of 1X model and the rest, still it looks like if the frequency would have been the same the lift forces would have been quite nearer. Though the lift may not be exactly equal to the 1X model, as the clapping effect is more pronounced in the 1X model, leading to sustaining of lift even in the upstroke (discussed in the PIV results), but yet the peak of maximum lift forces in the downstroke of other wings owing to their bigger span supersedes the 1x model provided they are at the same frequency of flapping. But due to effective clapping by the relatively smaller wing the net lift increases with decreases in wing size. Thus the effect of frequency is well pronounced on the lift produced. The average lift or the net lift can be increased by decreasing the negative lift generated in the upstroke (by effective clapping) or by increasing the positive lift in downstroke. Former way can be achieved by relatively smaller wing (as the relation of size and clapping is already discussed in PIV results) and hence by more effective clapping, whereas the latter way is achieved by increasing the frequency or to be precise by increasing the tip velocity and hence the Re.

It is quite evident from Fig 3.8 and 3.9 that thrust don't show similar response to wing size and frequency as that of lift. It increases in the same way for all the wings irrespective of the range of frequencies that they are operated with. It can be seen that for the same range of frequencies of 1.5X and 1.75X, the thrust is more for 1.75X. This indicates that it is more a function of tip velocity, thus on the combination of frequency and span both. As discussed in the PIV results that thrust forces are predominantly generated during the stroke reversals. Hence the magnitude of thrust is expected to depend on the vortex interactions during the stroke reversals. This depends on the

strength of the interacting vortices, which in turn depends on the tip velocities and hence on Re. thus with the same tip velocities and Re range the thrust generated will be similar. The same can be seen from Fig 3.8 and 3.10 where the thrust of 1.75X at lower frequency is almost equal to the thrust of 1X at higher frequencies. This is because the thrust depends not on frequency alone but wing span as well. So it's the product of both the parameters that determines the thrust. With more feathering effects of a wing, the contribution to thrust increases. This amount of feathering in our wings depends on the size as discussed earlier (it increases with wing size). Thus the thrust forces calculated for model 1 are more dependent on wing size than on the frequency. The same is also seen by the thrust calculations done by PIV data (Fig 3.11). So the behavior as shown in the force data is quite expected and verified for model 1 by comparing through the PIV data.

As the source and mechanism of generation of lift and thrust are different, hence their behavior and response to the parameters like frequency and wing sizes are different. As discussed in the PIV results that the lift depends on the tip velocity and the strength of vortices over it, as well as on the effective clapping it undergoes towards the end of the upstroke. So its dependence on the frequency becomes very prominent. Thrust is seen to be generated mainly during the stroke reversals due to the ejection phenomena. The strength of ejected jet does depend on feathering angle as well as the interacting vortices' strength which in turn here depends on the size of the wing and the tip velocity respectively for model 1. Thus thrust dependency with wing size is more observed than its dependency on the frequency. It is seen to be linear with wing span, whereas the lift dependency on the frequency is more dominant and here it is inversely varying with wing size (due to the effective clapping action).

Thus the nature of force data when justified with flow structures using PIV gives an idea of occurring mechanisms and the aerodynamics behind it. Even though the justifications and mechanism of flapping wing flight will change along with the type of wing, model or the forward velocity range (J range). But for the model used in the experiments in the unsteady regime with low Reynolds number, the basic aerodynamics is observed and noted out.

There exist some chances of errors in the force data calculated from the load cell experiments. As the whole model is placed over the load cell the motor vibrations or the hammer blow of the vibrating cg of the model which may not be eccentric with the column of the load cell. So due to all such unwanted factor the forces calculated from such experiments can be in the higher end. But yet the trend of such forces has to be the same. So if we are getting more values of the force than the actual that is produced by the wing itself then the measured value of forces will be towards the greater end in every experimental result. All the motor vibrations and eccentric effects will also grow with the flapping frequency. So the nature of variations of the forces produced actually by the wings will be the same as predicted here. Though the values may be a little different than what is shown, but the pattern and nature of the plots will still be same. Thus the conclusions inferred from the plots are quite reliable as its justified with the PIV analysis.

Apart from the force calculated from the load cells, forces are also calculated from PIV results (Fig3.11). As PIV gives velocity data in a plane, knowing the position of the wing momentum analysis can be done easily in a control surface surrounding the wings. This will give the forces in that particular plane. By taking 2D (two dimensional) assumptions forces over the wing are estimated. Though this will be a rough estimate as the actual flowfield is highly 3D (three dimensional), but here, as we are interested in the pattern and nature of the force, this rough estimate will even benefit our understanding of the flow physics over such flapping flight. As there is no forward velocity the thrust generated can be given as

Thrust (N) = ρAU^2 ……(1.7)

Where ρ is the density of air (1.225kg/m^3), A is the frontal area (wing span*thickness), U is the root mean square velocity in the wake profile.

Thus the thrust variation along a cycle is calculated through the data extracted from PIV results for both 1.75X and 1X, and are plotted in Fig 3.21. As per the assumption the cycle starts with downstroke thus till 0.56t/T on the time scale is downstroke and the rest is upstroke. Thus during the ejection after this point a significant thrust is expected and it is verified by Fig 3.21.

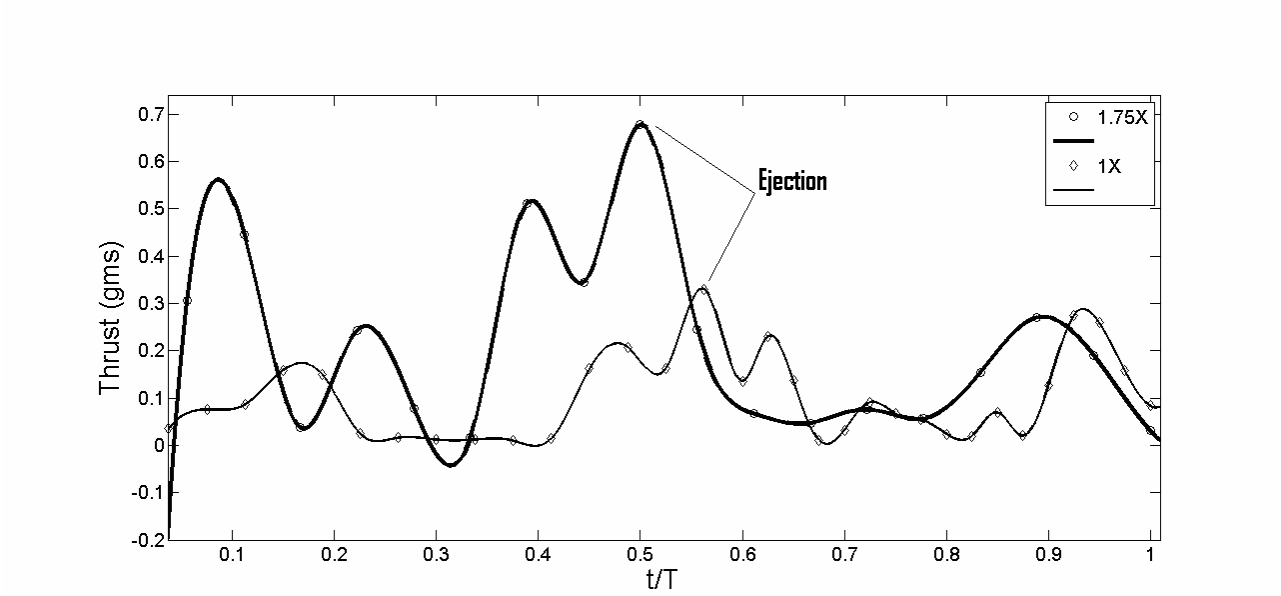

Figure 3.11 Thrust variations along time for model 1 using PIV data

As predicted in the PIV results that the time of shedding is delayed for the 1X wing due to its lower feathering angle as well as due to the staying of the TEV a little longer than 1.75X, the same can be seen from the Fig 3.11 where the thrust maxima for 1X model is delayed than the 1.75 X model. Here it is well seen that the total and average thrust is more with the increase in the size of the wing. Thus the PIV results are in perfect agreement with the load cell data.

Model 2 Results

The model 2 with forced feathering is not put directly onto the load cell. But yet the force estimation of the thrust is done using the PIV data momentum analysis as discussed for model 1. The thrust variation looks very smooth and the effect of shedding at both the stroke reversal points is well observed. The nature of the thrust generation is also similar.

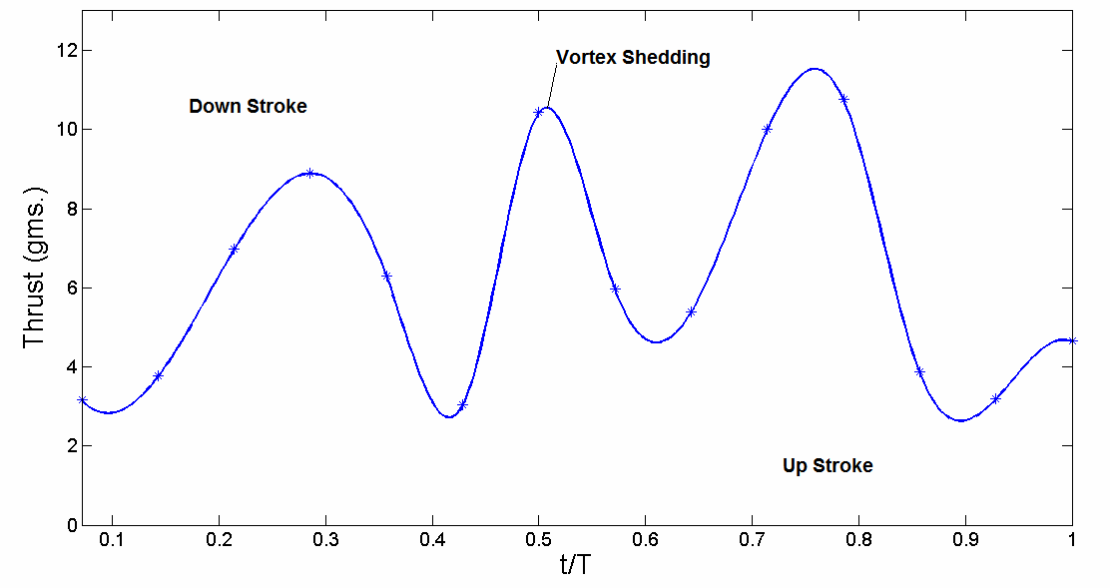

Figure 3.12 Thrust Vs t/T (For Model 2)

Model 3 Results

Only lift measurements are done for this model to view the effect of lagging. The experimental procedures and load cell being the same, only the new model is placed on the load cell and all other procedures are same. The effect of lead lag motion is observed from Figure 3.13-3.15. Only 1.75X wing is tested on the model.

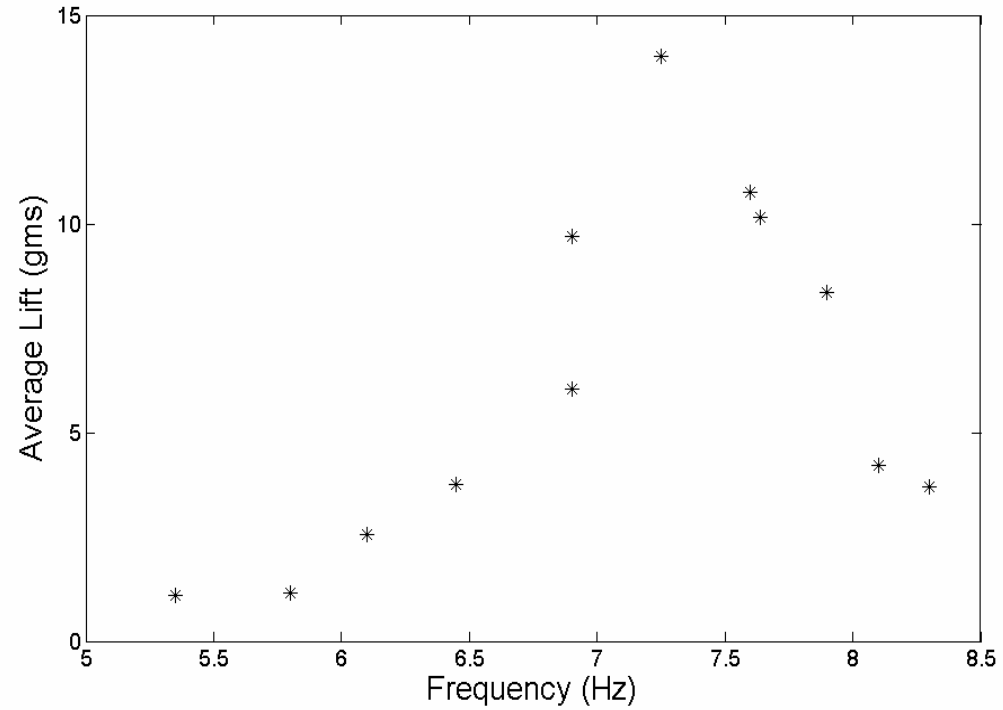

Figure 3.13 Average Lift Vs Frequency (For Model 3)

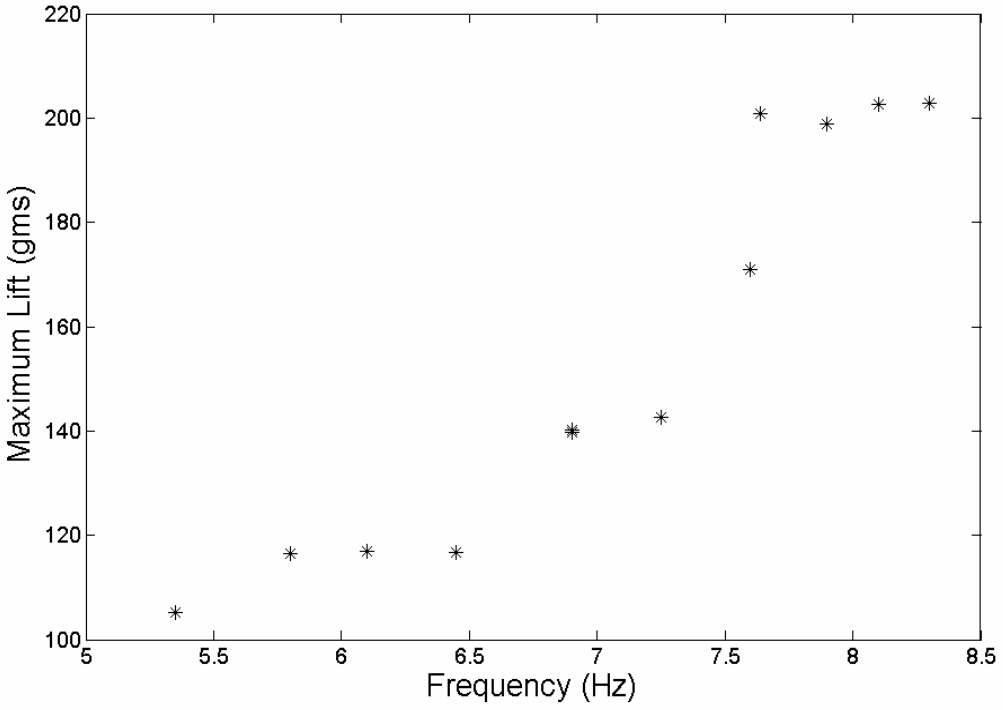

Figure 3.14 Maximum Lift Vs Frequency (For Model 3)

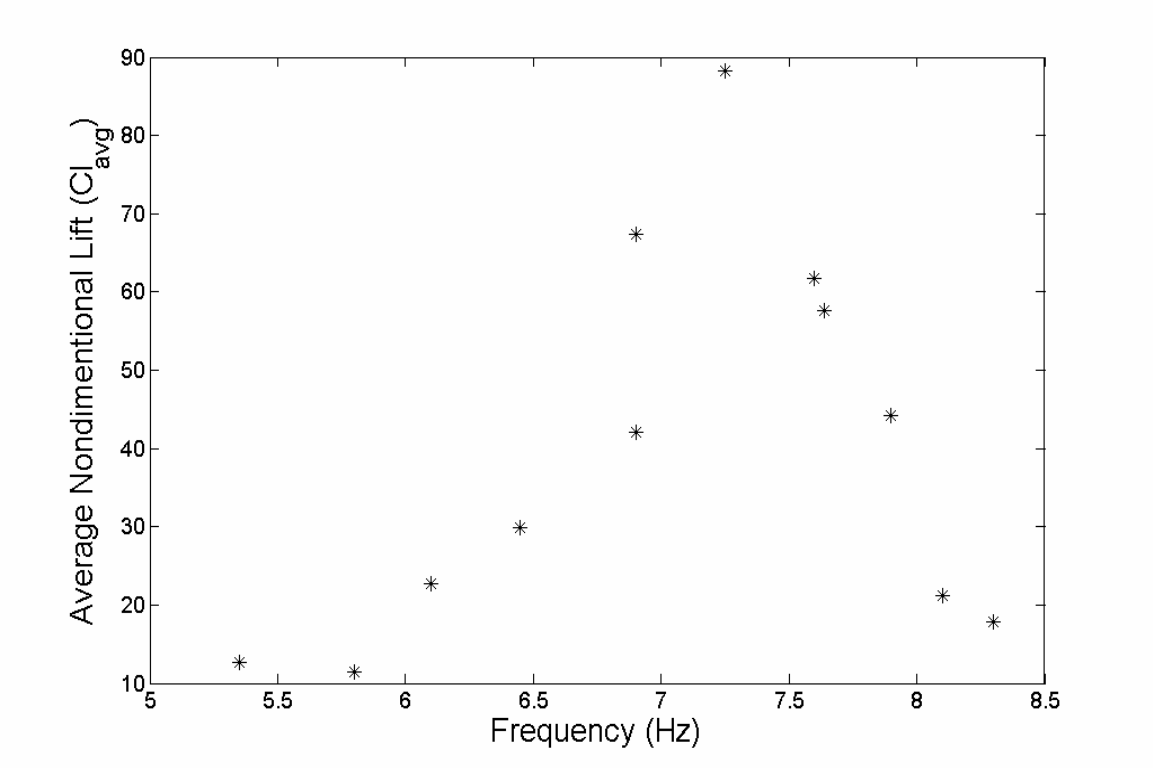

Figure 3.15 C_L avg Vs Frequency (For Model 3)

Here with model 3 even with no clapping action average lift is produced through lead lag motion. It can be seen that there is some detrimental effect of lagging motion on lift over a certain frequency range. The lift increases initially with the frequency just like the model 1 case. But after attaining a peak it decreases again. This gives some optimum value of the frequency for a particular size of the wing used. Going by these data, the optimum frequency is supposed to be around 7-7.5Hz which is quite in agreement with the butterfly flight where most of the species have around 6Hz frequency of flapping.

FLOW VISUALIZATION RESULTS

Extensive visualization experiments were carried out to understand the complex unsteady flow structures during flapping motion. Periodic clap and fling motion of the wing is associated with vortex formation around the entire wing edge and ejection of vortex rings The aim of the flow visualization here is to provide more insights towards understanding the role of vortices in generating aerodynamic lift and thrust. Experiments have been carried out in a water tank, with size (150cmsX50cmsX75cms). The experimental arrangement is shown in Fig 2.9-2.10. Fluorescent dye has been used for tracing the fluid path. Dye was injected before the start of the flapping on the wing in suitable positions.

Shape and size of single wing model used for flow visualization is shown in Fig 3.16. The flapping frequency of the model is 0.46 Hz. The total angle of flapping for this wing is 60^0 and the wing is started from a position 10^0 away from complete clap. The

visualization sequence given above shows some critical features during transition from upstroke to downstroke and vice-versa.

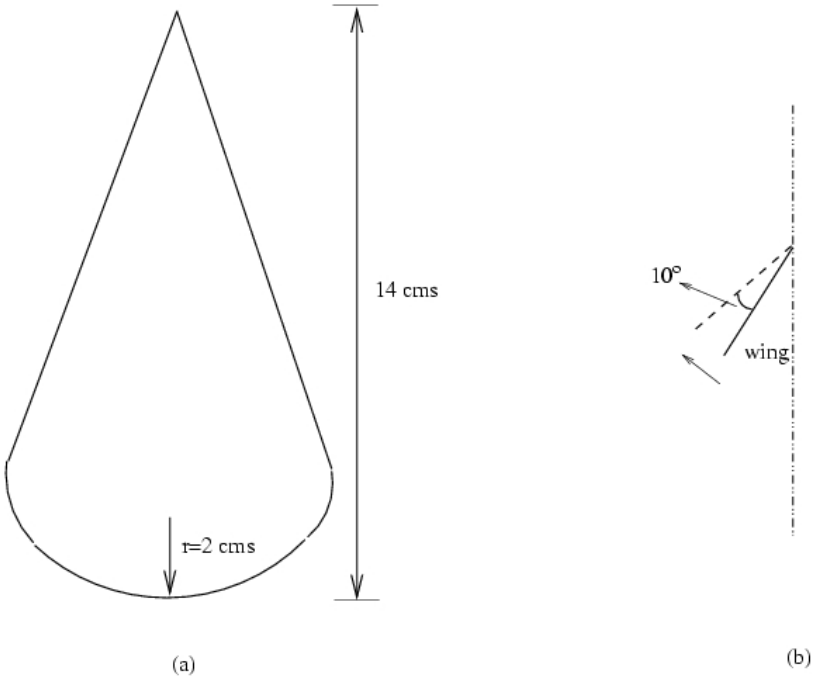

Fig 3.16(a) Dimensions of the symmetrical wing (b) wing at the starting position

In Fig 3.17 (a), the motion has just started towards left (marked as face A). A vortex, say (V_1) has rolled up on the leading edge of face B as expected. The vortex has grown with time as can be seen in the subsequent pictures (Fig 3.17(b)-(d)). In Fig 4.2(d), wing has just started moving towards right. As soon as the wing starts moving in an opposite direction, a small vortex is formed on the face A of the wing. Interaction of this vortex V_2 with the vortex V_1 forms a mushroom shaped vortex pair Fig 3.17(f) which is then ejected at an angle. These two vortices (LEV pair) are formed during the start of the downstroke. The interaction between these two vortex rings formed around the wing, and its movement in an angular direction w.r.t. the wing is mainly responsible for the unusually high lift generated by insects (butterflies). We have observed similar structures during the fling-motion for a double wing, when the total angle of the fling is approximately 60^0. In (g) we can see a residual vortex remains on face B of the wing, which rolls over to face A of the wing in subsequent motion. In (i), breakdown of the vortex structure which was been ejected has been observed. However, a portion of initial vortex has rolled over to the other side of the wing (Fig 3.17 (h), (i)) and is being dragged along in the downstroke motion. Since the wing is re-utilizing this vortex (as it was created in an earlier stroke), this phenomenon is known as '*Wake Capture'*. The vortex is known as the stopping vortex. Wake capture increases the size of the stopping vortex as seen in (i), (j) and (k). In (o), the wing has started return the stroke after completing the stroke described from (d)-(n). Vortex is again being ejected at some angle during the return.

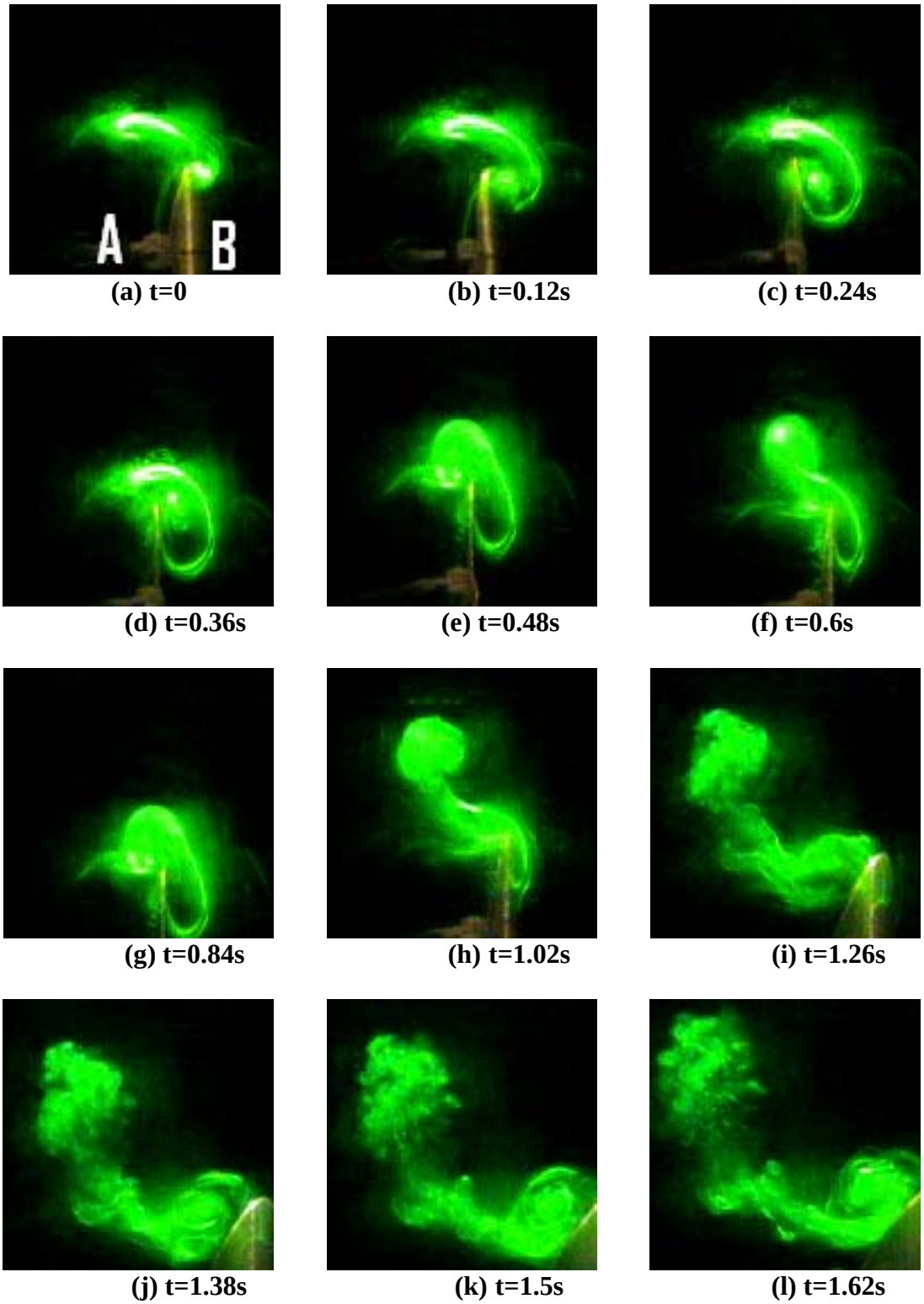

(a) t=0 **(b) t=0.12s** **(c) t=0.24s**

(d) t=0.36s **(e) t=0.48s** **(f) t=0.6s**

(g) t=0.84s **(h) t=1.02s** **(i) t=1.26s**

(j) t=1.38s **(k) t=1.5s** **(l) t=1.62s**

Fig 3.17 Vortex shedding visualization series (f=0.46Hz, symmetric single wing, span=14cms)

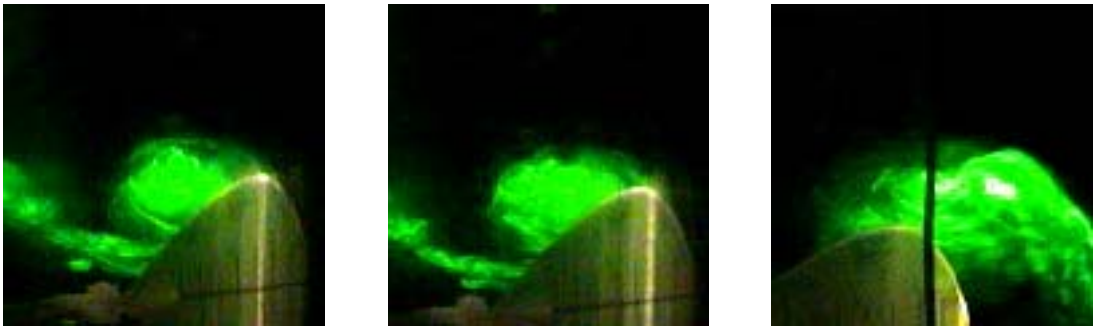

(m) t=1.74s **(n) t=1.86s** **(o) t=1.98s**

Fig 3.17 Vortex shedding visualization series (f=0.46Hz, symmetric single wing, span=14cms)

Thus the leading edge vortex and other vortex interactions as shown already in the PIV results are also observed with an elliptical wing of other dimensions. Thus the vortex dominated flow features are a common phenomena for flappingwing type flight provided they are in the same Re range and the timing and levels of interaction and behaviour of these cortex pairs do depend on the wing material and its flexibility.

4.Conclusions

PIV and force measurements are carried out to understand the aerodynamics of flapping flight, particularly butterfly flight. Various models with flapping wing and added features like feathering and lagging are used for experiments. The effect of the different models owing to their overall flapping mechanism is observed. The variation of forces and flow field with wing size, frequency or model as a whole is studied. In the force measurements section the dependence of aerodynamic forces (lift and thrust) for model 1 over frequency and wing size is shown in Fig 3.5-3.10. The nature of generation of these forces their respective timings in the cycle and occurrence of the key events leading to these peak forces have been justified by PIV results. The total flow sequence and the dominating characteristic of the flow, vortex structures and their mutual interaction are depicted in Fig 3.1. The effect of wing span or flapping frequency on the key events of force generation and the impact with their variation is also discussed. The key events like ejection, shedding of vortex pair, wake capture; LEV evolution is depicted in the PIV results. The same events are also observed in the flow visualization with elliptical wings in water tank showing the events as a general flapping wing phenomena in the particular Re range.The dynamics of such flapping motion is captured and various key events are pointed out in sequence of the presented data. The force data is in agreement with the predicted behavior from PIV analysis. The flowfield is better understood and the unsteady effects creating significant changes in the force generation and the parameters affecting them have been shown (like feathering angle and frequency for ejection). The effect of lagging is studied separately on lift force using model 3. Though PIV is not done on the model 3, still force results gives better idea about the effect of lagging on the lift and thrust variation (Fig 3.13-3.15). Forces (thrust) are calculated from the PIV results by

using momentum analysis and the nature of the forces is much in accordance to the results from the force measurements using load cell.

5. Future Work

Better models are now designed on a miniature level with even more degrees of freedom that can have a better control over the rotational twist at the stroke reversals and the overall lead lag motion followed by the wing tip. Stereoscopic PIV and Time Resolved PIV (TRPIV) experiments will give better insight of the nature of the wake and other unsteady effects present in the flow. The stereoscopic version of TRPIV will be able to show the nature of 3-D wake and flow field and will be able to measure aerodynamic forces with better accuracy. Oil tunnel measurement will carried out in near future. At present the tunnel is under construction. Force measurement techniques have to be refined and more sophisticated mechanisms, which will mimic an insect to a greater degree, have to be designed. The wing tip of the insects inscribes an ellipse during a single stroke. One has to study the variation of this inscribed ellipse and arrive at an optimum ellipse shape, as it is indeed an important factor for thrust production. The maneuvering can be studied in details other than the lift and thrust generation once proper model nearly mimicking a particular insect is ready. Force generations in such unsteady regime is complicated the maneuvering and the control over it will also take sufficient amount of work and effort to be well understood.

References

- Srygley R.B, Thomas A.L.R , 2002, "Unconventional lift generating mechanism in free flying butterflies" *Nature*; **420**, 660-664
- Ellington C.P, Van den Berg C, Willmott A.P, and Thomas A.L.R, 1996 "Leading edge vortices in insect flight" *Nature*; **384**, 626-630
- Dickinson M.H, Lehmann F.O and Sane S.P, 1999 "Wing rotation and the aerodynamic basis of insect flight" *Science*; **284**, 1954-1960
- Philips P.J, East R.A, Pratt N.H, 1981 "An unsteady lifting line theory of flapping wings with application to the forward flight of birds" *Journal of fluid mechanics*; **112**,97-125
- Ellington C.P, 1999 "The Novel Aerodynamics of Insect Flight: Application to Micro Air Vehicles." *J experimental biology*; **202** 3439-48
- Bomphrey R.J, Lawson Nicholas J, Harding Nicholas J, Taylor G.K, Thomas A.L.R, 2004 "The aerodynamics of Manduca sexta: digital Particle Image Velocimetry analysis of the Leading Edge Vortex" *J experimental biology*, **208**, 1079-84
- Sane S.P, 2003, "The aerodynamics of insect flight" *Journal of Experimental Biology* **206**, 4191-4208

List of Publications:

Debopam Das, Saurav K. Ghosh and C. Lakshmana Dora, On Three Dimensional Flow Field of Butterfly Flight, Proceedings of the Indo-US Workshop on Micro Air Vehicles 13-14 November 2008, Bangalore, India

Saurav K. Ghosh, Chandrala L. Dora, Debopam Das, Flow Field of Butterfly Flight: A PIV Study 8TH INTERNATIONAL SYMPOSIUM ON PARTICLE IMAGE VELOCIMETRY - PIV09 Melbourne, Victoria, Australia, August 25-28, 2009

Saurav K. Ghosh, Chandrala L. Dora, Shasant Anand and Debopam Das, Understanding the Role of Unsteady Vortices in Butterfly Flight through PIV Measurements 10th asian symposium of visualization December 7-10, 2009.

Manpower: Current: One Sr. Project Mechanic and One Project Associate. One Ph. D. Student (Partially Supported)
Previous: Two Students with M. Tech (For Two months, Partal Support)

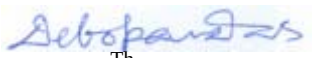

Date: 28Th Oct 2009.

Debopam Das; Ph. D.
Associate Professor
Department of Aerospace Engineering
Indian Institute of Technology Kanpur
Phone: +91 512 259 6163 /7227 /8578
Email: das@iitk.ac.in, debopam_d@yahoo.com